Comprehensive analysis of ship induced waves by means of field and computational methods

Hajók keltette partközeli hullámok átfogó elemzése mérési és numerikus modellezési módszerekkel

TDK 2015

by
Gábor Fleit

Supervisor
Dr. Sándor Baranya

Co-supervisors
Dr. Tamás Krámer
Dr. János Józsa

Department of Hydraulic and Water Resources Engineering
Budapest University of Technology and Economics

Budapest, 2015

Abstract

The inland navigation is clearly one of the most environment-friendly manners of transportation, however, it can also have negative effects on e.g. the riverine habitat. Investigations related to this topic are of great importance and provide research topics for several different disciplines. The more studies in these topics published, the clearer that the proper treatment of these problems cannot be handled from a single aspect, interdisciplinary approach is required, where e.g. civil engineers, biologists, ecologists and ship engineers work together. Such a joint work, however, requires the most advanced investigation methods of each participant.

This study deals with the hydraulic effects of ship induced waves near the river bank, with a special focus on near-bed flow. The local increase of the bottom shear stress, generated by ship induced waves, might detach macroinvertebrates and fish eggs from the substrate which can easily be lethal for them. Foreign studies show that the ecological aspects of the problem are manageable, but the understanding of the complex hydraulic phenomena still calls for further research.

In my previous study, different field measurement techniques and data analyzing methods were tested to prove their applicability for such investigations. Acoustic Doppler Velocimeters (ADV) were deployed to investigate the dynamic changes in near-bed flow velocities, furthermore a novel application of the Large Scale Particle Image Velocimetry (LSPIV) was also presented to analyze the surface velocity characteristics of breaking waves near the river bank. In this study both the field methods and data analysis procedures have been improved based on the experiences gained in the previous study, moreover, a new device (Aquadopp) has also been deployed which is designed to measure three-dimensional velocity profiles along verticals. As a significant improvement compared to the previous studies, the field data have been used to parameterize and validate a 3D Computational Fluid Dynamics (CFD) model, which provides a more detailed insight in the complex hydrodynamic phenomena.

Recently, a feasibility study was prepared connected to the chosen study section in the Danube River, which aimed at the protection of the river bank against the impact of ship induced waves. The artificial formation of a gravel bar was proposed in that study. Such an island could provide a safe habitat for macroinvertebrates and would serve as a safe spawning site for fish as well. Due to the lack of suitable investigation methods, the influence of the gravel bar on the waves could not yet been quantified. However, utilizing the 3D CFD model (REEF3D), capitalizing the computational capacity of the supercomputer at BME

(Superman), a significant step could be made towards the analysis of wave dynamics in such a complex bed geometry.

The results will be used to perform sample applications of ecohydraulic analysis as well. Such examples greatly support the further joint investigations with biologists.

Tartalmi kivonat

Mára már nem kérdéses, hogy a hajókkal történi áru- és személyszállítás napjaink egyik legkörnyezetkímélőbb fuvarozási formája, mindazonáltal az esetleges káros (pl. élőhelyre kifejtett) hatások nem hagyhatók figyelmen kívül. Ezen hatások felderítése és különböző aspektusokból való vizsgálata aktuális és releváns kutatási téma számos tudományág keretein belül. A témában született tanulmányok alapján egy dolog kijelenthető: a hullámjelenségek hatásának átfogó vizsgálatához és a problémák megoldásához több tudományág képviselőinek összehangolt munkája szükséges, vagyis interdiszciplináris megközelítés szükséges, melyben pl. építőmérnök, ökológus, halbiológus, hajómérnök együtt dolgozik. Ehhez azonban az egyes feleknek legjobb tudásuk szerint kell megvizsgálni a saját szemszögükből fontos hatásokat és következményeket, továbbá elvárásként fogalmazandó meg a legmodernebb mérési és adatfeldolgozási módszerek alkalmazása is.

Jelen dolgozatban a hajók keltette hullámok partközelben megjelenő áramlástani hatásait vizsgáltuk, különös tekintettel a mederfenék közeli áramlási viszonyokra. A hullámok okozta megnövekvő fenéksúrlódás pl. hatással van a mederfenéken élő makrogerinctelenekre, valamint a halak ívóhelyére. Túl nagy fenék-csúsztatófeszültség értékek esetén pl. ezek az élőlények elsodródhatnak olyan nagy áramlási sebességek uralta területekre, ahol túlélési esélyük zérushoz közeli. Külföldi tanulmányokban már található példa a probléma ökológiai szempontú vizsgálatára, de mérnöki szempontú célirányos áramlástani vizsgálatok alig állnak rendelkezésre, hazai szinten a kutatási téma pedig egyértelműen hiánypótló.

Tavalyi TDK dolgozatomban megvizsgáltam, hogy a rendelkezésünkre álló mérési és adatfeldolgozási módszerek hogyan állíthatók szolgálatba ilyen elemzésekhez. Akusztikus Doppler-elvű sebességmérő műszerekkel (ADV) vizsgáltuk az áramlási sebességek dinamikus változását a mederfenék közeli rétegben, továbbá a Large Scale Particle Image Velocimetry (LSPIV) képfeldolgozáson alapuló eljárás egy újszerű alkalmazása is bemutatásra került, mellyel az part közelébe érkező és ott megtörő hullámok felszíni sebességviszonyait elemeztük. A tavaly szerzett tapasztalatok alapján mind terepi mérések kivitelezését, mind az adatfeldolgozási eljárásokat továbbfejlesztettük, valamint egy új, korábban még nem használt, sebességprofil mérésére alkalmas műszer is bevetésre került. A vizsgálatokat továbbá kiegészítettük numerikus áramlástani modellezéssel is, melynek segítségével még egy lépéssel közelebb kerültünk a hajók keltette hullámzások áramlástani hatásainak megértéséhez.

Az esettanulmányként kiválasztott folyószakasz partközeli szakaszának védelmére készült tervek szerint egy kavicspad kerülne megépítésre, mely mérsékelné a hajók keltette

hullámzások káros hatásait, így biztonságos élőhelyet nyújtana a mederfenéken élő makrogerincteleneknek valamint a halak számára is stabilabb ívó helyet biztosítana. A mű kedvező hatásának számszerű értékelésére korábban nem volt lehetőségünk, most azonban egy új, a hullámok mozgását is szimulálni képes számítógépes áramlási modell, valamint a BME szuperszámítógépének (Superman) munkába állításával erre is lehetőségünk nyílt.

Az előállított eredményeket felhasználva élőhely szempontú mintaalkalmazásokat mutattunk be, mellyel felkínáljuk a közös vizsgálatok lehetőségét a témát gondozó biológusok számára is.

Acknowledgements

This study is a sequel of research activity from the past two years at the Department of Hydraulic and Water Resources Engineering of the Budapest University of Technology and Economics (BME)., therefore I would like to express my gratitude in general to everyone who participated and/or helped me in my scientific investigations.

I owe special gratitude to Dr. Sándor Baranya, for his continuous encouragement and support in the past two years, and for his supervision over my work in many interesting and flourishing research topics.

Special thanks is given to Dr. Tamás Krámer for his conductive advices regarding the analysis of the field measurements, and for intruding me to the basics of linear wave theory and to wave related flow phenomena in general.

I would like to express my sincere gratitude to Prof. János Józsa, who provided the financial background for the field measurements and I am also thankful for him inspiring and supporting my work at the department.

I would like to thank Károly Tóth and István Pozsgai technicians for helping us to successfully conduct the field measurements, and for building the required stands and accessories for the instruments.

I want to express my gratitude to Péter Torma PhD candidate for his help in the very first deployment of the Aquadopp device, which resulted in success, valuable data were gathered.

The work reported in the paper has been developed in the framework of the project “Talent care and cultivation in the scientific workshops of BME” project. This project is supported by the grant TÁMOP-4.2.2.B-10/1—2010-009.

Contents

1 Introduction

Inland navigation is clearly one of the most environment-friendly manners of transportation, however, it can also have negative effects. In fact, the available knowledge concerning these effects (mechanical damages caused by propellers; oil contaminations; questions related to the stability of ecosystems and the decrease of biodiversity; effects of navigation motivated river trainings; effects of ship induced waves etc.) is increasing and it is still considered to be an up-to-date research topic for a wide range of scientific disciplines (biology, chemical engineering, mechanical engineering, environmental engineering, civil engineering etc.). The more studies in these topics have seen the light, the more it become clear that the proper treatment of these problems cannot be handled from a single aspect, interdisciplinary approach is needed. Such a joint work, however, requires the most advanced investigation methods of each participant.

In present study, the effect of ship induced waves in a Hungarian section of the Danube will be investigated in detail from the aspect of hydraulic engineering, with special focus on near-bed flows. The relevance of research in this area is unquestionable considering that the Danube is the second largest river of Europe, thus one of the most important navigational routes of the continent as well, which also leads to its emphasized role in the Water Framework Directive of the European Union.

The hydraulic engineering community has already started to take the first steps to understand more about the different effects of navigation, especially from the aspect of hydrodynamics, but the understanding of the complex hydraulic phenomena still calls for further research. The theoretical background required to describe different types of waves is well-developed, but the implementation of these methods for natural situations is far from trivial. Ship induced waves describe complex wave systems especially in heterogeneous morphological surroundings, moreover, in natural environments the wave characteristics depend not only on the shape of the river bank, the water depth and the morphological properties of the channel, but on the speed, size, shape and draught of the ships as well. These recognitions have made it clear, that in order to understand the appearing phenomena (flow and wave related features), detailed field measurements have to be carried out, preferably in various environments and conditions. Studies conducted in sections of the Austrian Danube showed that different wave theory related parameters and characteristics of these complex wave systems can be evaluated based on data acquired by proper field measurements (*Krouzecky et al, 2013*). Moreover, ecohydraulic results have also seen the light, larval drift was estimated by the exposing of drift nets near the shore to collect fish being swept into the current (*Liedermann et al., 2009*).

Local increase of bed shear stress – generated by ship induced waves – has serious impact on fish eggs, juvenile fish and macroinvertebrates living in, on or close to the river substrate. Increased shear stress can detach individuals from their natural habitats, which is lethal in most of the cases. Foreign studies reported that the ecological aspect of the problem is manageable (*Gabel, 2012; Kucera-Hirzinger et al., 2009*), however the hydraulic point of view has not yet been revealed in detail.

The field measurement and data processing methods employed in present study, had been improved and developed based on experiences acquired during previous filed investigations on the very same study site (*Fleit, 2014a*). This way, not only better quality data was obtained, but the results were more suitable to support numerical investigations as well.

Computation Fluid Dynamics (CFD) is getting more and more frequently employed for the solution of hydraulic engineering related problems. These numerical models usually mean a less time and cost demanding alternative against the classically used physical models. Numerical models most frequently used by the industry are simple one-dimensional solvers, which are well applicable for the simulation of flood waves. Due to their simplicity they are very fast, therefore able to provide significant time advantage for flood protection.

Two- and three-dimensional models are rather applied for tasks with more complex flow conditions (e.g. flow around structures). Because of the numerical and mathematical complexity of these solvers, the use of such models is often limited by the available computational capacity. The rapid development of computer sciences also leads to the advancement of CFD, not only the previous tasks become easier to solve, but new interesting topics arise as well, such as the simulation of breaking waves in the near-bank zone of a river. The proper numerical treatment of these complex conditions requires the employment of CFD models with up-to-date numerical methods.

Open-sourced numerical model REEF3D was employed in present study, which is a good alternative compared to expensive commercial software. The model consists of up-to-date numerical methods, high-order discretization schemes and advanced free surface capturing methods. The software is under continuous development and testing, however, its capability for stable treatment of different types of free surface flows, waves and even breaking waves have also been reported (*Chella et al., 2015 Afzal et al., 2015; Fleit, 2015*).

This study aims to investigate the hydraulic and ecohydraulic effects of ship induced waves, by up-to-date filed measuring and data processing methods. Methods have been upgraded compared to previous studies, detailed data analysis was conducted in order to characterize the different wave events from the aspect of hydraulic engineering, and a sample application

is also presented to make the first major steps towards interdisciplinary research. Numerical model REEF3D was utilized to prove the reproducibility of ship induced waves with significantly simplified geometry and boundary conditions in a two dimensional slice model. The validated 2D model provided with the opportunity to fulfill a three dimensional impact analysis of an artificial gravel bar which had been designed to protect the littoral zone and the bank of the selected section of Danube River, consequently would provide a safer and more stable habitat for local aquatic creatures.

2 Study site

The studied river reach is a backwater between two groins in River Danube (around rkm 1675, Hungary). This is the area of Sződliget, the Szentendre Island is on the right, Sződliget is on the left bank of the river. Approximately two-third of the total discharge of the Danube goes through this river arm, consequently the arm is used as an inland navigational route. Fluvial navigation, not only can have harmful effects on the ecosystem of the littoral zone, but ship induced waves might be responsible for bank erosion as well.

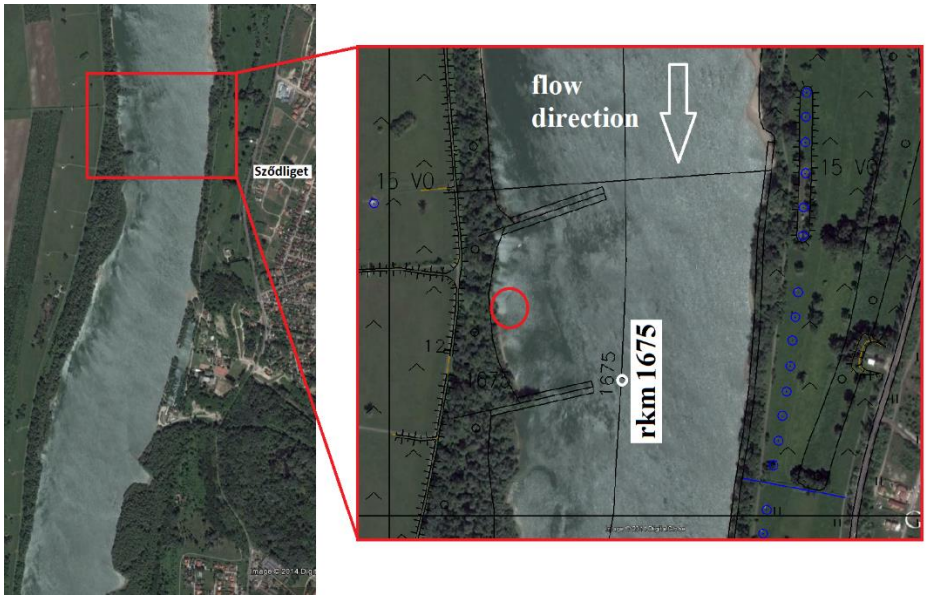

Figure 2.1 – Study site

In order to ensure safe navigation on the river, two pairs of groins are located in the area. Field measurements were carried out between the northern pair of groins, in the littoral zone (**Fig. 2.1**). These river training works make the study site both hydraulically and morphologically complex.

2.1 Planned river trainings

Plans had been created to improve the ecological potential of the studied reach with special focus on native fish species. Design alternatives were prepared in the area of both groin pairs, to achieve a better, more suitable environment for the ecosystem of the river reach (**Fig. 2.2**):

- Northern area
    - Increasing flow velocities near the bank by tearing down the first 25 meters of the structures (measured from the touchline) and aggravating this zone of the river bed as well.

- Creating a place between the structures which is protected from ship-induced waves in order to facilitate better reproduction and growth rates by building an artificial gravel bar with slight slopes. This should protect both the fish seeds and the different macroinvertebrate animals (nutrition of the juvenile fish) from detachment related to waves.

- Southern area
  - The idea there was to create a short tributary on the left bank, which would be a bypass around the southern groins. Since this intervention is supposed to improve the quality of riverine habitats on the study reach as well, its tracing had been designed with the consideration of the geometrical characteristics of natural rivers. It was designed to provide at least 1 m of water depth at all times, even at low water conditions. The longitudinal profile is a sequence of pools and riffles, which is reported to be a good quality habitat due to the provided diverse flow conditions (*Pasternack et al., 2008*).

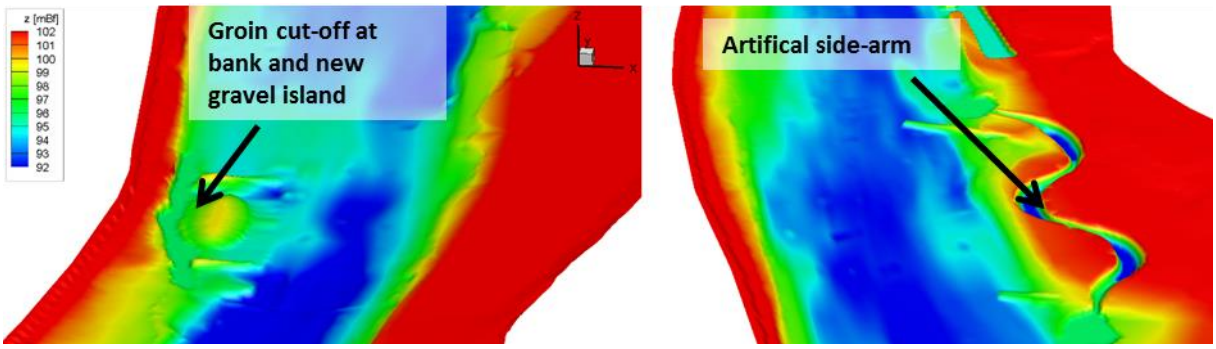

Figure 2.2 - Planned river trainings in the area of the northern (left) and southern (right) groin pairs (*Fleit, 2014b*)

The study site had been investigated with up-to-date field measurements and data processing methods, to find out more about the hydraulic and morphological characteristics of the area and to test the applicability of ecohydraulic methods for the Hungarian Danube (*Fleit, 2013*). These results provided a good base for later three-dimensional numerical modeling, which was required to fulfill a detailed impact analysis (*Fleit, 2014*) and further ecohydraulic investigations. Sedimentation engineering methods were employed to assure that the modifications do not affect the navigational route in an unfortunate way (*Józsa et al., 2014*). These studies provided with a lot of useful data and experience, however the helpful effect of the gravel bar for the macroinvertebrates and juvenile ships could not have been evaluated, at all. One of the main aims of this study is to make up for the lack of these investigations.

3 Field measurements and instruments

3.1 Acoustic Doppler velocimetry

There is a wide range of modern measurement devices and instruments available for different tasks of hydraulic engineering. Most of the up-to-date velocity measurement devices exploit the Doppler effect which is the change in frequency of a wave (or other periodic event) for an observer moving relative to its source. The shift of frequency is proportional with this relative velocity. The device emits acoustic pulse of high frequency which is reflected from particles (e.g. suspended sediment) floating in the water volume (and moving with its velocity). The reflected signal is received by the device, the velocity can be calculated based on the frequency shift. The relationship between the change of frequency and the flow velocity is the following:

$$f_{Doppler} = 2 \cdot f_{source} \cdot \frac{v}{c} \tag{3.1}$$

where $f_{Doppler}$ is the frequency shift at the receiver, f_{source} is the frequency of the source sound, v is the relative speed of the particle and c is the propagation speed of sound in water.

In the following sections two Doppler-based instruments will be presented, which were deployed during the field measurements.

3.1.1 Acoustic Doppler Velocimeter (ADV)

The ADV employed in present study (**Figure 3.1**) is a fairly small device, which was basically designed for lacustrine conditions and laboratory experiments. Considering that the flow velocities generated by ships are relatively low, and that the measurements were conducted in shallow water, the field deployment of the device was found to be safe.

Because of its fixed geometry, the ADV samples approximately 1 cm^3 of the water volume which comes from the segment of the emitted acoustic pulse and the received echo therefore, it can be said the device is suitable for sampling a single point of the water volume.

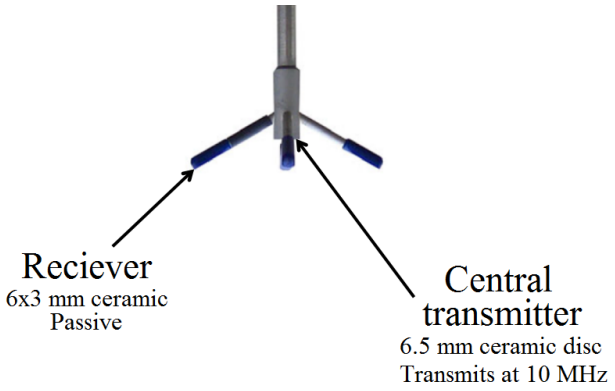

Figure 3.1 – The Acoustic Doppler Velocimeter (Vectrino)

The ADV was attached to a steel rod which was stuck in the substrate firmly. In order to prevent the undesirable movement of the device, the rod was further stabilized with a tripod which is normally used as a stand for geodesy surveying devices.

The device was used with a sample rate of 16 Hz and was set to sample a point of the water volume right above the river bed.

3.1.2 Aquadopp High Resolution (HR) profiler

The Aquadopp measures the column current profiles using the acoustic Doppler technology as well. The device is designed for a wide range of applications from coast to rivers, it is a small, lightweight, and cost-effective solution for shallow water (<100 m) deployments. In contrast with the ADV devices, the Aquadopp is designed to measure velocities in the whole water column above (or under) its position.

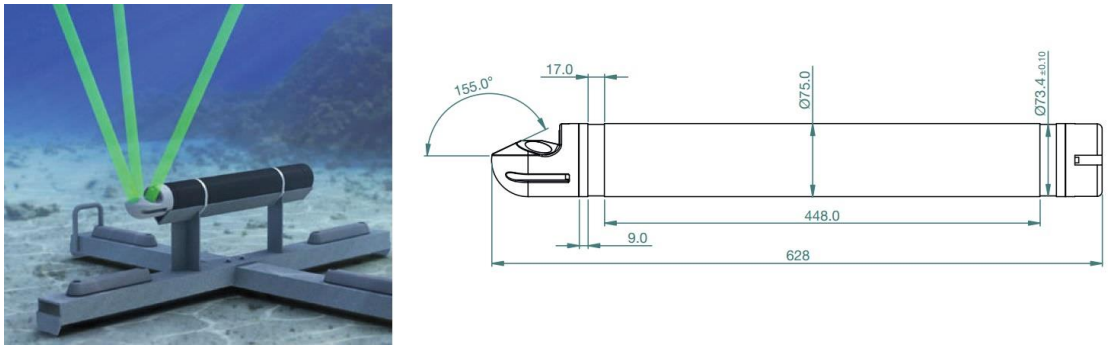

Figure 3.2 - Aquadopp High Resolution profiler (*Nortek, 2013*)

The instrument employed in present study is an Aquadopp High Resolution (HR) profiler. The HR firmware upgrade turns the Aquadopp Profiler into a high resolution profiler operating at sub-cm scales with sampling rates as fast as 8 Hz. The device also includes a pressure gauge, which is almost indispensable when dealing with wave related phenomena.

The device has a blank zone of 14 cm relative to the echo sensor. In this zone, no measurements are done. The Aquadopp was deployed similarly to **Fig. 3.2**, but was located as close to the substrate as it was possible. The device was used on the maximal sampling rate of 8 Hz.

3.2 Video recordings

The measurement setup was completed with a Full HD video camera (GoPro 4), which was fixed on a stable stand right above the touch line. The camera has a wide-angle lens (fish-eye optic), so it was suitable for recording the approaching and then breaking waves on a relatively high area. These records were later processed and analyzed with Large Scale Particle Image Velocimetry (LSPIV).

Figure 3.3 – GoPro HERO4 camera

The LSPIV is an up-to-date picture processing based method, which was developed to conduct quick and easy discharge measurements in rivers. It is able to calculate two-dimensional surface velocity vector fields based on nothing else but video records. The method, however, requires some kind of a pattern or patch to detect and follow in order to operate properly. In present case, this was the foam appearing due to wave breaking. The applicability of the method for dynamically changing flow features, such as waves had been in question at first, but previous tests and results reported that the method is suitable for quantifying the propagation velocity of the approaching waves (*Fleit, 2014*a).

Improvements were also applied to the field application of the method:

- The camera was fixed higher than last time and it was also positioned in an angle in order to capture a larger area. The new setup increased to usable area for calculations from 5-10 m^2 to up to 100 m^2.
- The legs of the stand were also positioned differently than before, so they are not visible in the records. It was found that if there are static objects on the picture sequences, then the calculations around them are likely to be loaded with errors. This upgrade provided with better quality results.

The theoretical background of LSPIV and the process of the whole method will be presented in detail in Chapter 4.

3.3 Field measurement campaign

Field measurement campaign had been planned and then carried out in order to obtain fair amount data for the detailed analysis of ship induced waves, and to support numerical modeling as well. The deployment of the instruments had been improved based on previous experiences, which resulted in better quality data. GPS measurements were conducted to gain accurate elevation data for the river bed of the littoral zone, which is vital for setting up a correct digital terrain model (DTM) for the numerical simulations. In addition to the

measurements, a substrate sample was also collected, which grain size distribution was later analyzed in a laboratory, and was used to parametrize the bed roughness of the numerical model.

The field measurements were conducted on 16th July 2015 in a low water condition. The deployed and employed instruments were the following (**Fig. 3.4**):

- Acoustic Doppler Velocimeter (Nortek Vectrino)
- Aquadopp HR Profiler (Nortek)
- GoPro camera
- Real Time Kinematic (RTK) GPS device
- Substrate sampler

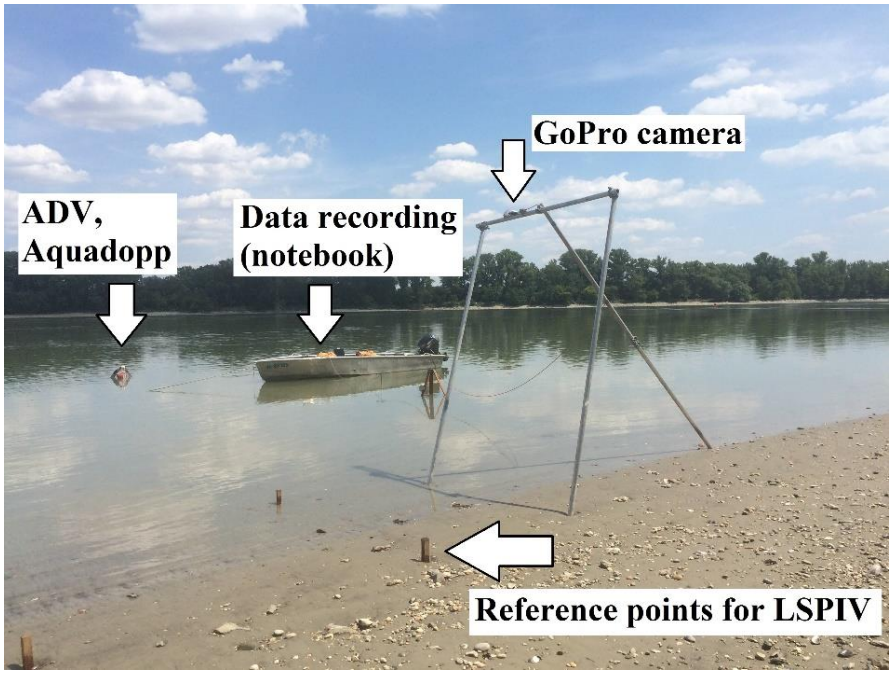

Figure 3.4 – Field measurement setup

Table 2.1 presents the type of ships which passed the study site during the field campaign, with their direction included. In the following sections, ships will be identified by the time they passed.

Table 2.1 – Ships passed during the measurements

Time	Type	Direction
13:06	hotel ship	downstream
14:01	hotel ship	downstream
14:49	barge	downstream
15:00	hotel ship	upstream
15:23	hotel ship	upstream
15:43	hotel ship	upstream

4 Data processing

4.1 Analysis of the near-bed velocity measurements

The analyzing method used to evaluate the three-dimensional velocity time series obtained with the ADV had also been improved. Since this device is able to continuously operate on the sampling rate of 16 Hz, the measurements are randomly loaded with erroneous data. These problematic data points contain unlikely high velocity vectors, especially compared to the neighboring ones.

A very simple and straightforward way to filter these series is to simply remove these salient data by giving a maximal absolute accepted velocity, and whatever exceeds this limit is to be removed. The problem with this method is that it is not necessarily able to filter erroneous data if there is a wide range of velocity fluctuations in the time series, because a limit determined to the higher magnitude data will probably not work for lower magnitude velocities.

Because of this deficiency, slightly more advanced methods need to be employed. Since the ADV devices are very widespread and can be utilized for many different causes, several methods had been developed to filter the erroneous measurements from the time series. However, it was found that most of these methods had been developed for the measurement of quasi-permanent flows, which can be characterized with a single averaged velocity vector. This meant a huge limitation when looking for the most appropriate filtering method, nevertheless, a very simple and effective technique was found to filter these dynamic, highly time-dependent velocity time series.

The time-series were filtered based on the quality of the measure signals, which can be characterized by the correlation of the signals and with the Signal to Noise Ratio (SNR). Both parameters are recorded at every sampling for all four beams. The data filtering was conducted with the introduction of a correlation limit (70 %) and a SNR limit (20 dB) recommended by the manual of a signal analyzer software developed specially for Nortek devices (*Jesson, 2015*). Note that in the following figures, velocity vectors are presented in a compass-like coordinate system (North and East are for the positive velocity values). The main flow direction of the river in the studied section is from North to South, the wave related velocities are expected on the orthogonal axis (East - West).

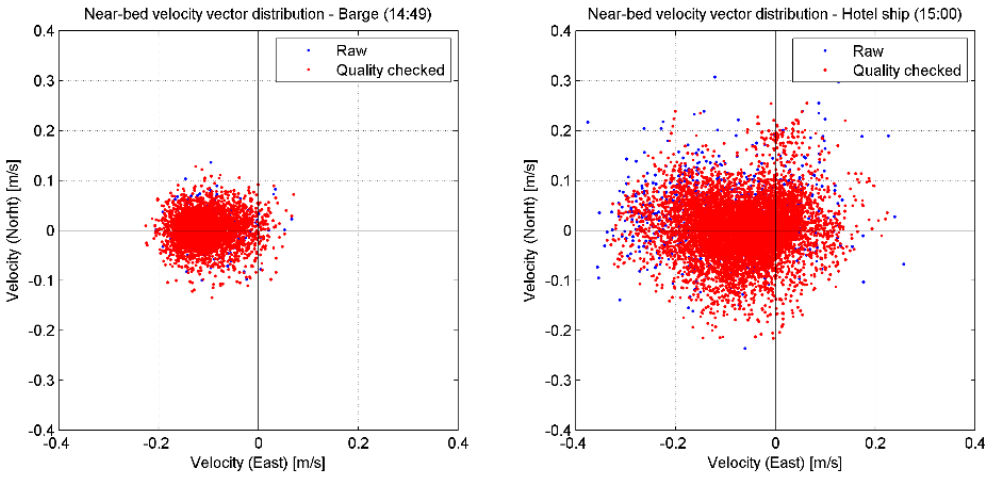

Figure 4.1 – Raw and quality checked horizontal, near-bed velocity distributions

A trend of approximately 10 cm/s is observed in **Fig. 4.1**, in the direction of the bank. Previous years' ADCP measurements were examined to find the explanation of this irregular background current in the backwater of the groins (**Fig 4.2**).

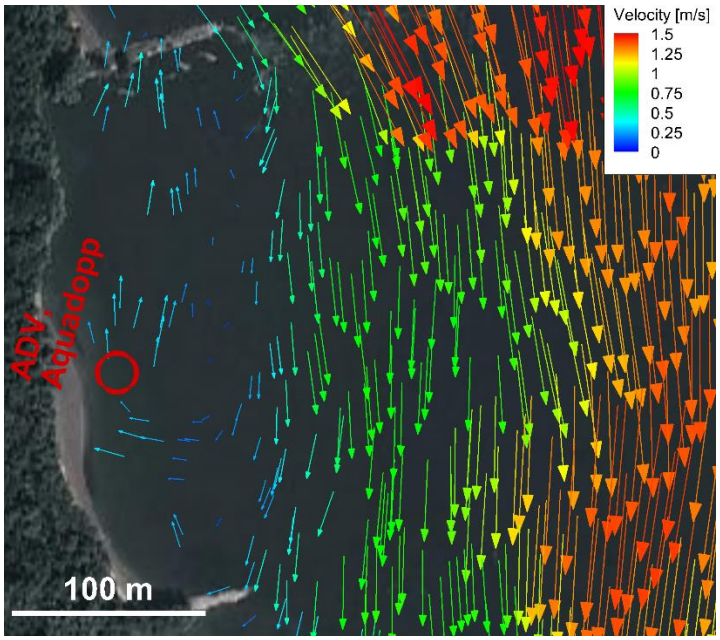

Figure 4.2 – Interpolated, depth-averaged velocity vector field and the location of the instruments (*Fleit, 2013*) and the location of the instruments in present study

Note, that the velocity vectors on **Fig. 4.2** belong to a bit higher water condition from two years ago, therefore it is not a perfect representation of the condition at present investigations. It is observed, that the direction of the background flow is opposite to the main flow direction at the location of the instruments. However, the turn back of the current is observed in approximately 10 meters distance, where the velocity vectors point in the direction of the bank, similarly to what is present in the measured data (**Fig. 4.1**). In absence of further proof,

it is assumed that the lower water level might move the turn back point northward which explains the trend observed in the velocity measurements. However, it is noted that the scientific foundation of this statement would require further investigations.

In order to complete further analysis on the velocity time series, the trends had to be eliminated. The velocity series were detrended, which resulted in velocity scatters with a center of gravity in the pole of the coordinate system.

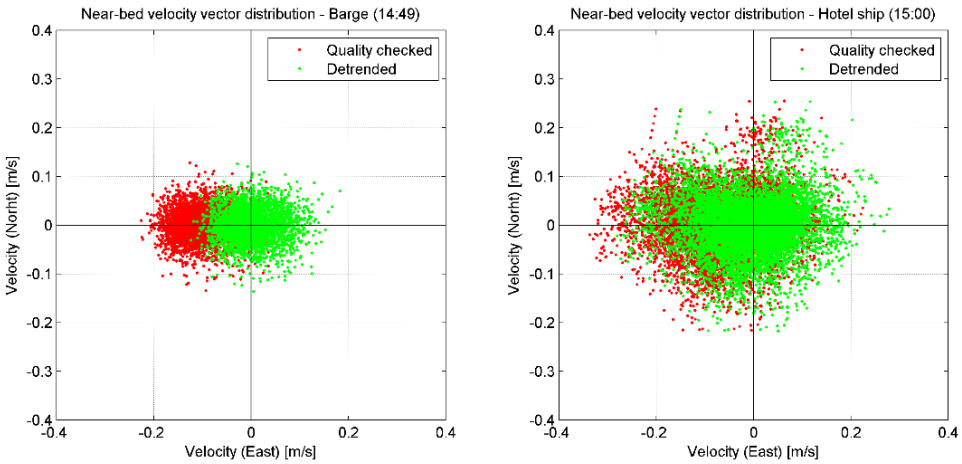

Figure 4.3 – Detrending of the horizontal, near-bed velocity distributions

Although, the ADV was deployed with an orientation in which its *X* axis (East) was looking in the direction where the waves are expected to approach from, this does not necessarily mean, that this direction overlaps with the main direction of wave generated flows. In order to convert the values of the possibly correlated horizontal velocity components (u, v) into a set of values of linearly uncorrelated variables with and orthogonal transformation, the filtered time series were examined with principal component analysis (PCA) (*Jolliffe, 1968*). PCA results in a transformation matrix wherewith the original velocity vectors can be transformed in the coordinate system determined by the principal components.

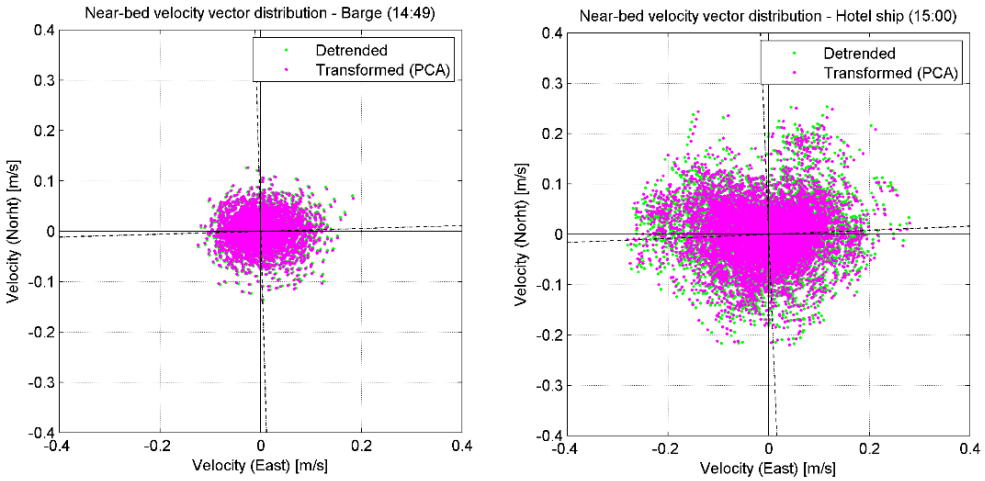

Figure 4.4 – Transformed velocity vector distributions

Fig 4.4 presents velocity distributions transformed into the original coordinate system determined by North as the *Y* and East is the *X* axis. The direction of the principal component was transformed into the East axis as it was approximately assumed to be the main direction of ship generated velocities. The detrended scatter is also shown (green) with the principal directions calculated with PCA (dashed).

Connection between the principal direction of ship generated flows and the advance direction of different ships was examined. In order to do make the comparison clear as possible, not only the principal directions are shown in the following figure, but a schematic figure of two ships with opposite directions are presented as well with their waves, which imply the expected principal directions (**Fig. 4.5).**

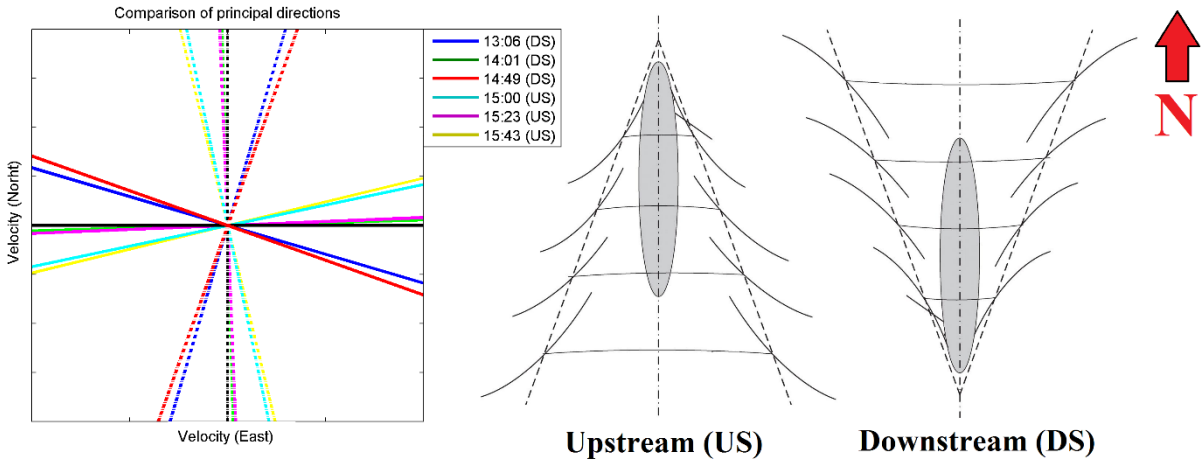

Figure 4.5 – Principal flow directions (solid line) for different ships in comparison with the North-East coordinate system (the dashed lines are the directions for the lowest correlations)

Schematic figures of the ship waves presented above make it quite clear what is the expected direction of the waves, however the plotted graph shows almost the exact opposite of that.

Pcipal components for ships 14:01 and 15:23 show minimal deviation compared to the base direction (East). However, for ships moving in downstream direction (13:06 and 14:49), the axes rotate in the direction where the upstream headed ship waves are expected. The same contrary is observed for upstream head ships 15:00 and 15:43). Scientifically grounded explanation was not found for the phenomena. It is noted, that the groins complicate the hydrodynamic and morphological characteristics of the study sight in general, therefore it is possible that they also significantly affect wave related flows, so they behave in such unexpected ways.

The velocity time series obtained by PCA (velocities in the principal direction, u_p) were further analyzed via discrete Fourier transformation (DFT) to define the spectrum of the velocity time series. Note that the spectral density was weighted with frequency when plotting the following graphs.

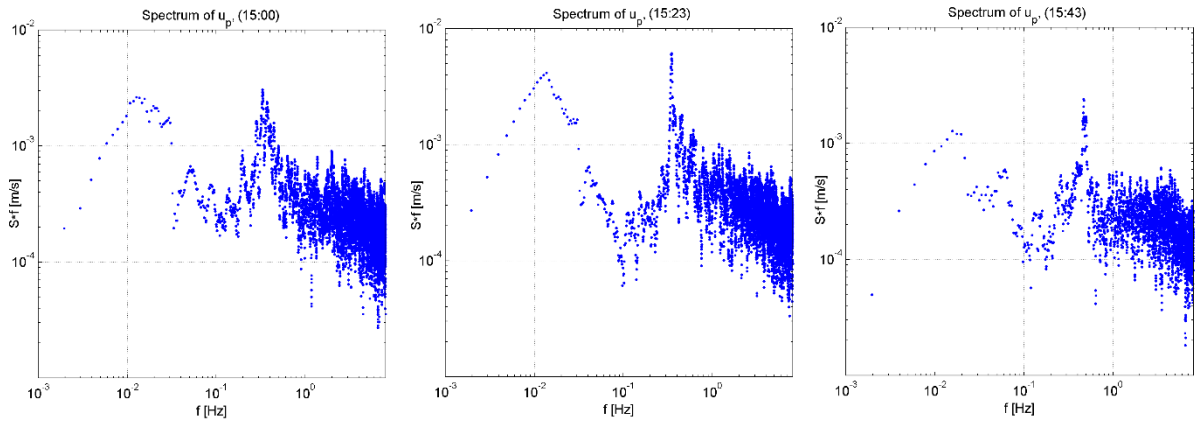

Figure 4.6 – Spectrum of u_p for three ships (spectral density weighted with frequency)

Interesting characteristics are observed on **Fig. 4.6** for ship generated velocities: two peak values are observed for frequencies of different magnitudes. The first peak appears around wave period of 60 - 90 seconds, the other one is at 3 - 4 seconds. These results show that ship induced waves are generally superimposed from two significant wave frequencies.

It is noted, that these characteristics also appear in the analysis of the pressure measurements. The high frequency waves are the ones we observe easily on the bank after a ship leaves, the low frequency waves are not necessarily observed on steep sloped river bank. However, in case of lower slopes it can appear as a slow motion of the touch line up to a displacement of meters. The latter was the case for the field campaign, this kind of motion of the touchline was observed, and recorded with the video camera. The extremes of a two minutes long section are presented in **Fig. 4.7**.

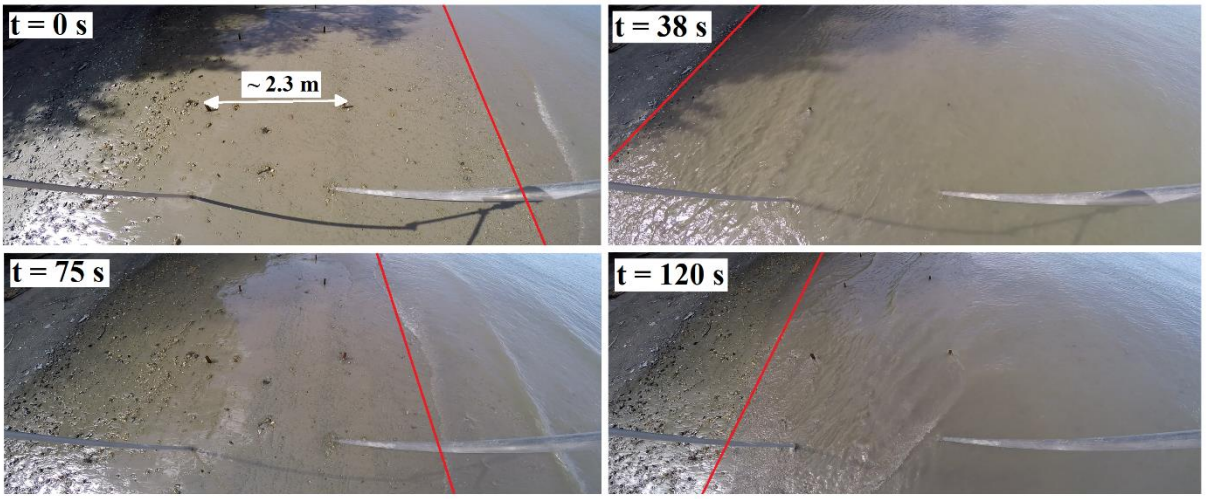

Figure 4.7 – Touchline (red) displacement due to slow waves, in a two minutes long section (15:23), the red line is skew due to the fish-eye optic

The touchline is emphasized with red, because it cannot be seen clearly from the photos on their own, due to the wetted parts of the bank which is not under water at the moment. The video records had to be used to define the location of the touchline, where its movement was easily traceable. Wave period of approximately 75 seconds is observed on **Fig. 4.7** which matches with the low frequency period observed on the spectrums of the velocity measurements.

Time series of wave related velocity time series (u_p) were smoothened to eliminate the effect of turbulent fluctuations. This was achieved by the moving averaging of the results (**Fig. 4.8**) with a window size which preserves the main characteristics of the velocity series (based on spectral analysis). The main benefit of the smoothened time-series is that they are better and easier to compare with the results provided by CFD modeling and also make it easier to observe the flow features above the scale of turbulence. The utilized numerical model works with the Reynolds-averaged Navier-Stokes (RANS) equations, therefore turbulence is not represented directly, but with the introduction of eddy viscosity. The moving averaged results were used for bottom shear stress estimations and for the validation of the numerical model.

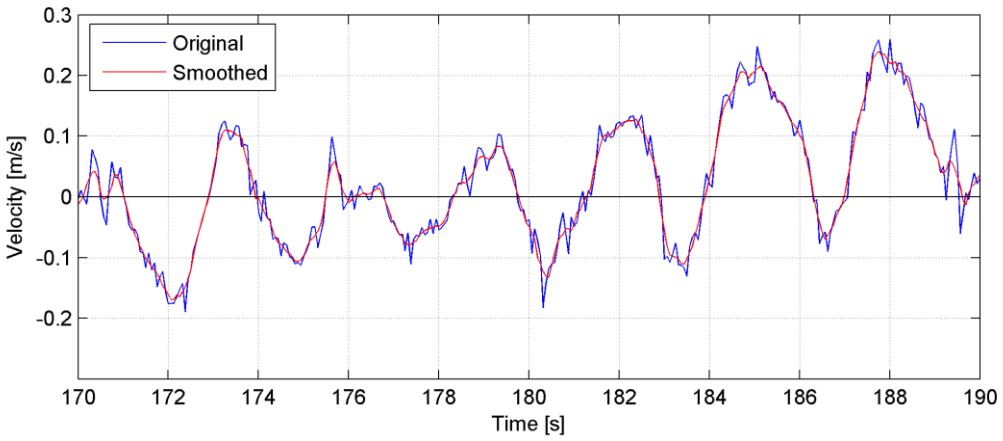

Figure 4.8 – Moving averaging of velocity (u_p) time series (section of a whole measurement)

The bed shear stress (τ_b) is proportional to the second power of the maximal orbital velocity at the bed (*Jonsson, 1966*), therefore it is one of the most important parameter, when estimating detaching forces due to ship-induced waves. Maximal near-bed orbital velocities were evaluated for 60 seconds long sections, to see the time dependency of this parameter, and to prepare it for bottom shear stress estimations (section 4.4).

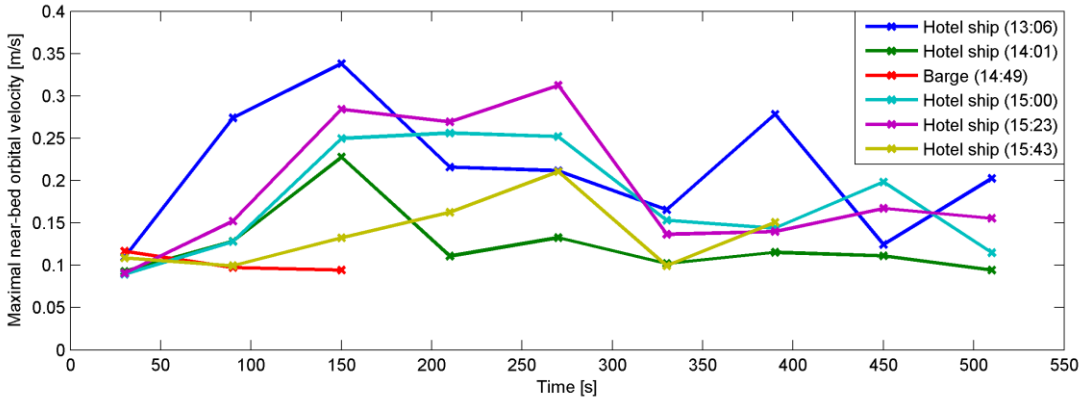

Fig. 4.9 – Maximal near-bed orbital velocities over time for different ships

4.2 Analysis of velocity profile measurements

The Aquadopp device was deployed on the river bed, however, the sampled section of the water column was limited by its stand, the geometry of the device, blank zones and the device's firmware as well (**Fig. 4.10**).

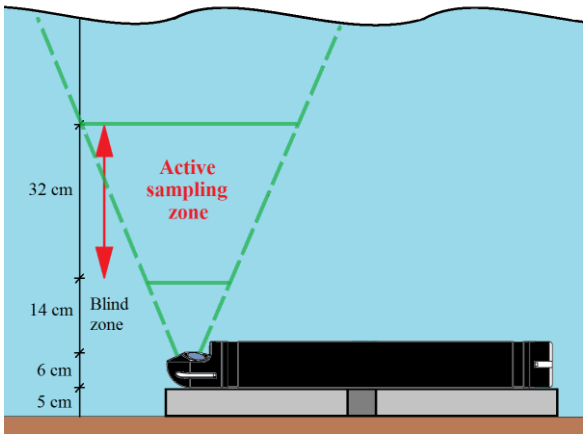

Figure 4.10 – Deployment of the Aquadopp device in present study

This field campaign was the very first deployment of the Aquadopp device at the host institute, therefore it has to be noted, that both its field application and the following analysis of the three dimensional velocity measurements require further developments in the future in order to obtain more valuable data. The main aim of its deployment in the present research project was to test the device and to meet its limitations.

Fig. 4.10 presents the active sampling zone of the device for the present study, which was divided into 8 even sections, so the instrument measured three-dimensional velocities in 9 points. The lowest point was at 25 cm from the bed, the highest was at 57. It has to be noted, that as the instruments measures velocities farther and farther from the device head, the bigger the distance will be between the three points sampled by the splayed beams, which leads to more spatial averaging, consequently, dynamic changes related to waves might get smoothened or even totally eliminated by the averaging. An example to this effect is presented in **Fig. 4.11**.

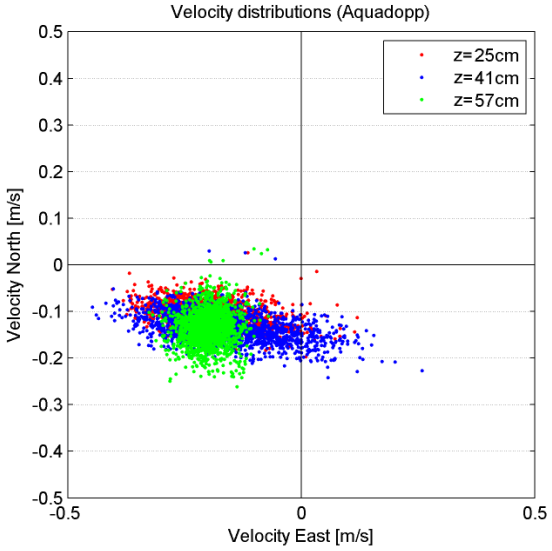

Figure 4.11 – Velocity distributions in different heights above the bed (14:49)

Note, that the figure above belongs to a barge (14:49), which representing the slightest wave event. Horizontal velocity distributions for the lowest, the highest and the middle layers are presented in the figure. Compared to the near-bed velocity distributions presented before, in addition to the trend in the direction of the bank, a trend of approximately 0.10 - 0.15 m/s is also noticed in southern direction, which means that the background current is an even more complex. Wave related velocity fluctuation appears in the bottom and middle layer's velocity distribution, however, these characteristics almost entirely disappear in the uppermost layer due to the previously mentioned spatial averaging. This recognition helps the proper planning of future field measurements.

Similarly to near-bed velocity time series, the Aquadopp measurements were also detrended and analyzed with PCA. Principal directions were calculated for all layers (different depths above the bed) to detect the complex spatial nature of ship generated flows between the groins. The principal components (solid line) and the related secondary, orthogonal directions (dashed) for two hotel ships are presented in **Fig. 4.12** for five different levels.

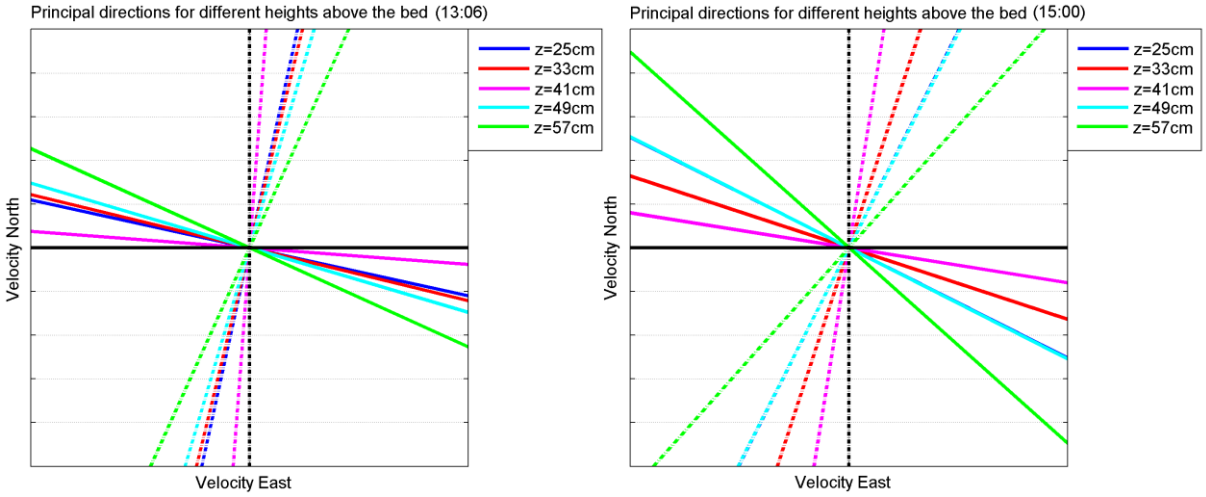

Figure 4.12 – Principal directions for different heights above the bed

Maximal deviation in the orientation of principal directions are up to 30 - 40° in the different levels. On one hand, this might be a result of the increasing spatial averaging moving away from the bed, but on the other hand it can also be a result of a secondary flow feature, which proves the three dimensional nature of flows under such complex conditions, and would call for the 3D numerical modeling of these phenomena as well. Although, it has to be noted, that the ships 13:06 and 15:00 caused much more intense wave events than the barge (**Fig. 4.11**), where this secondary flow feature is not that significant.

4.3 Analysis of pressure measurements

The analysis of the pressure measurements was conducted based on methods presented in *Homoródi et al.* (2012). Since ship induced waves show different characteristics over time, the pressure time series were not analyzed for the whole events (~ 10 mins), but for shorter (60 secs) series, all measurements were divided into 60 seconds long sections. The spectrum of the pressure $Z_p(f)$ was computed from the pressure time series using DFT, whereof the surface elevation $Z(f)$ was derived with the assumption of linear wave theory and zero phase shift (*Massel, 1996*):

$$Z(f) = \frac{Z_p(f)}{g\rho} \cdot \frac{\cosh[k(f)h]}{\cosh[k(f)(h - h_p)]} \tag{4.1}$$

where g is the acceleration due to gravity, ρ is the water density, h is the total water depth measured from the mean water level, h_p is the depth of the pressure sensor and $k(f)$ is the wave number of the wave component with frequency f, defined implicitly from:

$$(2\pi f)^2 = gk \tanh(kh) \tag{4.2}$$

Wave components of long and very short timescales were removed from each measurement. The long components were eliminated with a high pass filter (~ 0.15 Hz), the components from the timescale of turbulence were removed with a low pass filter (~ 9 Hz). It is noted, that these values were defined separately for all measurements. This filtering was necessary in order to make the compensated spectral density suitable for determining the bulk wave parameters (e.g. significant wave height). Cutoff frequencies were determined based on the spectral density of full measurements (~ 10 min) (**Fig. 4.13**). Note that the spectral density was weighted with frequency when plotting the following graphs.

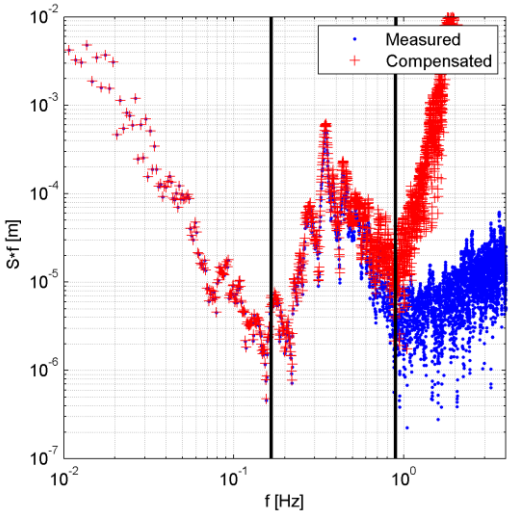

Figure 4.13 – Spectrum of the measured and compensated surface elevations and the cutoff frequencies (15:23)

Once the problematic frequencies were eliminated from the calculations, the pressure time series were divided into 60 seconds long sections. The spectrum of the compensated surface elevations was calculated for all sections in order to prepare the data for further calculations.

Useful parameters can be derived from the wave spectrum. In general, the i^{th} moment is defined by a frequency-weighted integral of spectral density:

$$m_i = \int_0^\infty f^i \, S(f) df \tag{4.3}$$

In the present case the integration was interpreted between the cutoff frequencies and the integral was numerically approximated for the discrete values with the trapezoidal rule for $i = 0, 1$. These moments then can be used for the calculation of different wave parameters as following:

The significant wave height is obtained from the moments:

$$H_{m0} = 4\sqrt{m_0} \tag{4.4}$$

The wave period corresponding to the average frequency of the spectrum is:

$$T_{m01} = \frac{m_0}{m_1} \tag{4.5}$$

The average wavelength is calculated by exploiting that $L = \frac{2\pi}{k}$:

$$\bar{L} = \frac{2\pi \int_0^\infty S(f)df}{\int_0^\infty k(f)\, S(f)df} \tag{4.6}$$

where the integration of the wave spectrum was also conducted with numerical integration on the discrete values.

The temporal distribution of these parameters made it straightforward to evaluate changes in wave phase speed for each ship as well, which will be later evaluated with LSPIV as well (section 4.5). In order to provide comparable data for the LSPIV, the average wave phase speed was calculated:

$$c_p = \frac{\bar{L}}{T_{m01}} \tag{4.7}$$

Temporal distribution of the presented wave parameters for different ships are presented in **Fig. 4.14 - 4.17**,

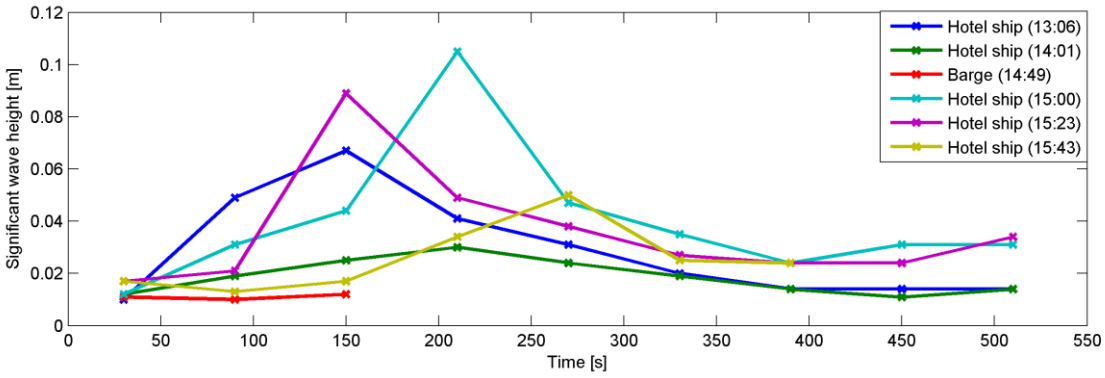

Figure 4.14 – Temporal distribution of significant wave height for different ships

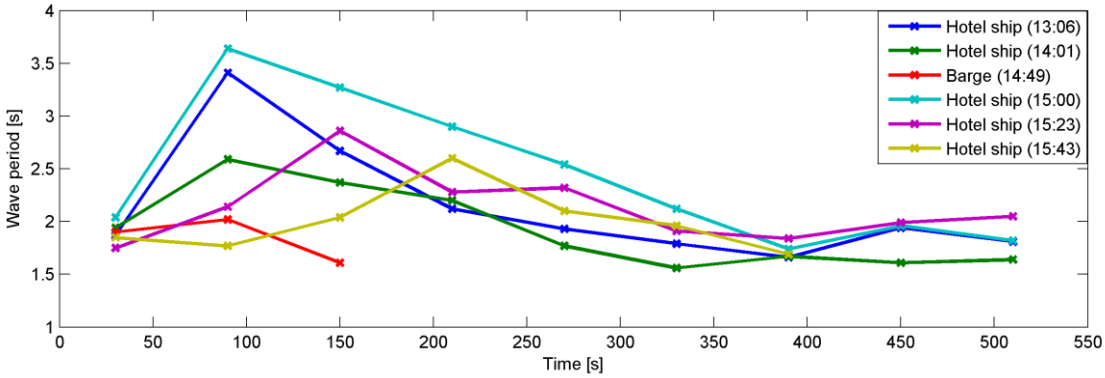

Figure 4.15 – Temporal distribution of average wave period for different ships

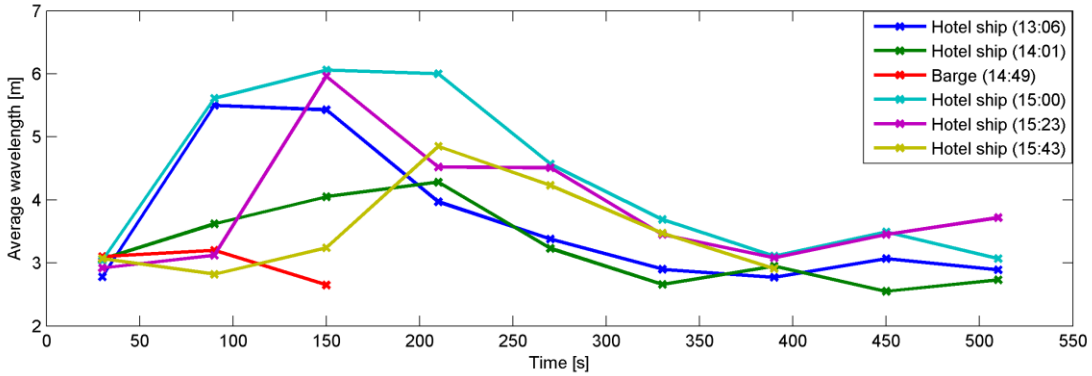

Figure 4.16 – Temporal distribution of wave length for different ships

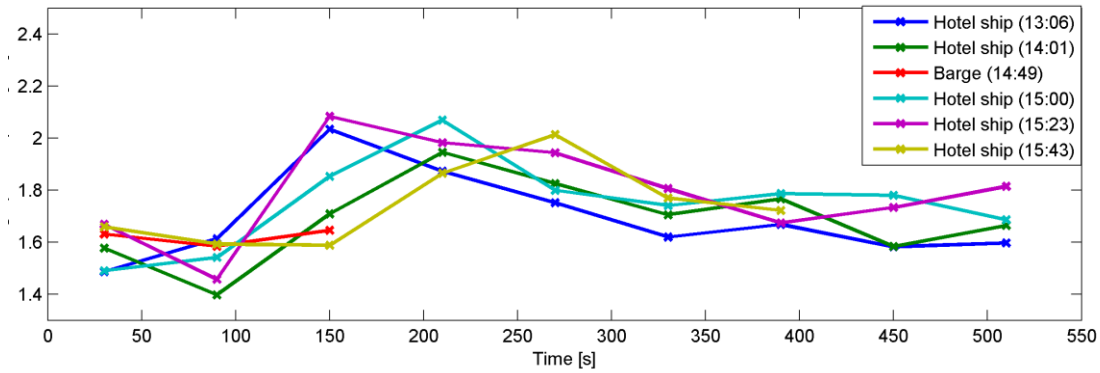

Figure 4.17 – Temporal distribution of wave phase speed for different ships

Based on the numbers, the hotel ships at 13:06, 15:00 and 15:23 were the most intense wave events during the measurements, which is fully confirmed by the experiences during the field campaign. It is noted, that the different parameters do not reach their maximal values in the same time. Wave period and wave length are usually the first ones to peak, the temporal distribution of these parameters is strongly related. Wave height reach their maximal values around 3-4 minutes, maximal significant wave heights are up to 10 cm for hotel ships 15:00 and 15:23. In general it is noticed, that hotel ships 13:06, 15:00 and 15:23 are the ones with the most intense wave events. Measurements related to the barge were terminated after three

minutes, because there was no noticeable wave event after its passing, which is supported by the calculated results as they show minimal change over time, and the values of the different parameters are also significantly lower than the other ones.

Far-reaching conclusions cannot and should not be derived from these results, however, the differences between ship induced wave characteristics do emphasize the relevance of further investigations, relationships between different ship related parameters (speed, draught, shape, load, etc.) and the relevant wave parameters need to be explored.

4.4 Estimating bottom shear stress

The most frequently used methods for calculating bottom shear stress in riverine conditions are deduced from turbulent velocity fluctuations and turbulent kinetic energy (*Soulsby and Dyer, 1981*). The employment of these methods for ship induced waves is, however, not trivial, because of the emerging high – not turbulent – velocity fluctuations, and spatial complexity of the related phenomena. Previous study (*Fleit, 2014*) reported that the wave related bottom shear stress cannot be properly evaluated from the turbulent kinetic energy, because Reynolds-decomposition is not unequivocal in case of such dynamic time series, different methods need to be employed.

The method used in present study evaluates bottom shear stress based on wave theory related variables. The bed shear stress (τ_b) is proportional to the second power of the maximal orbital velocity at the bed (*Jonsson, 1966*):

$$\tau_b^w = \frac{1}{2}\rho f_w {U_w}^2 \tag{4.8}$$

where ρ is water density, U_w is the maximal orbital velocity on the bed and f_w is the wave friction factor (*Pleskachevsky, 2005*):

$$f_w = 2\sqrt{\frac{\nu}{U_w A}} \tag{4.9}$$

where ν is the fluid viscosity (kinematic) and A is the semi-orbital excursion determined as

$$A = \frac{U_w T}{2\pi} \tag{4.10}$$

where T is the wave period.

This method results in a single value of shear stress, which is the maximum for the analyzed time period. Previous study (*Gabel, 2012*) reported, that the Jonsson-method is suitable for the evaluation of bed shear stress based on ADV data, moreover, its applicability for ecohydraulic purposes is also possible.

The method was previously used for calculating maximal bottom shear stress for whole wave events (*Fleit, 2014*). Since the characteristics of ship-induced waves might significantly change over time, the method might overestimate the overall effect of a wave event. In order to cure this disability, the bottom shear stress values were calculated for one minute long periods, based on the wave parameters evaluated previously in this chapter.

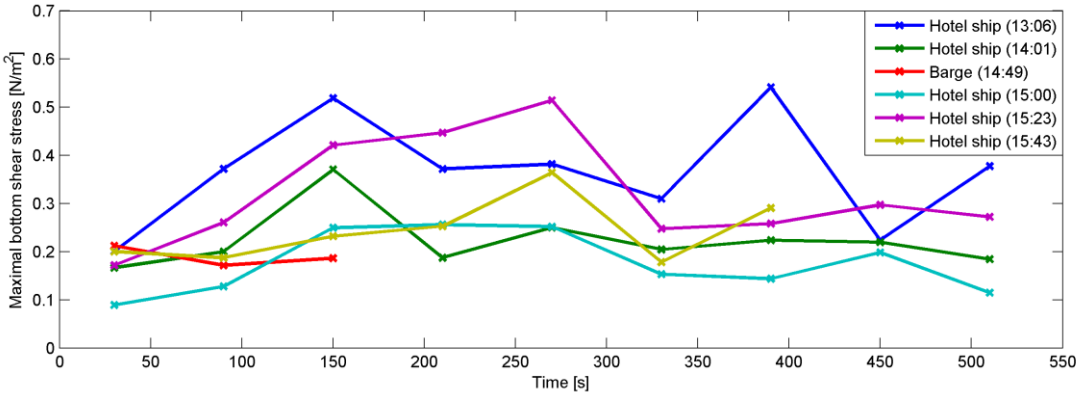

Figure 4.18 – Temporal distribution of maximal bottom shear stress for different ships

It is noticed, that bottom shear stress values do not have such a characteristic change over the time like the wave parameters did, which is explained by the fact that its value very much depends on maximal orbital velocities, which were also quite irregular. Since bottom shear stress is proportional to the second power of velocity, the shapes of the graphs are very similar to temporal distribution of velocities presented in **Fig. 4.9**. Previously, it was pointed out, that hotel ship 15:00 was responsible for one of the most intense wave events, but when it comes to detaching forces, the effect of the ship stays below average, which also proves the relevance of further investigations, with the inclusion of ship related parameters as well.

All data processing and analysis up to this point was completed with self-developed MATLAB scripts.

4.5 Large Scale Particle Image Velocimetry

4.5.1 Background

LSPIV is an up-to-date data processing method, which requires only video records, capturing the water surface to calculate two-dimensional (horizontal) velocity fields (e.g. *Muste et al., 2008*). The method was basically developed for fast discharge measurements in order to provide a cheaper and faster alternative compared to the classic methods and devices. The LSPIV identifies patches and patterns on the consecutive frames and evaluates their displacement, thus the velocity vectors can be calculated with the elapsed time between two

frames. The strength of the method lays in its simplicity and swiftness, its field deployment requires no more than a video camera.

In order to employ the LSPIV algorithm, the recordings were first broken into pictures, then had to be transformed to obtain a plain view orthogonal to the free surface. These transformations were conducted by the freely available Fudaa-LSPIV software (*Jodeau et al., 2013*) based on the reference points fixed during the field measurements:

$$i = \frac{a_1 x + a_2 y + a_3 z + a_4}{c_1 x + c_2 y + c_3 z + 1}$$
$$j = \frac{b_1 x + b_2 y + b_3 z + b_4}{c_1 x + c_2 y + c_3 z + 1} \quad (4.11)$$

where $[i, j]$ are the coordinates in the reference system of the pictures (in pixels) and $[x, y, z]$ are the real coordinates (in meters).

Once the pictures are transferred, the calculation parameters were defined. The following parameters had major effect on the quality of the results and on the solution time as well, hence their proper determination was very important.

- Size of the interrogation area (IA): the size of a rectangle [pixel^2] where the algorithm identifies patches and patterns.
- Size of the search area (SA): the size of a rectangle [pixel^2] where the algorithm searches for the patches and patterns identified in the IA.
- Time step size (δt): time step between consecutive frames. Required to evaluate velocities from the calculated displacements.

In order to perform the calculations, a grid has to be defined, where every gird point will be a center of an IA. During the calculations, the software evaluates the cross-correlation (R) between the patterns found in every IA and SA of the following frame:

$$R(a_{ij}; b_{ij}) = \frac{\sum_{i=1}^{M_i} \sum_{j=1}^{M_j} (A_{ij} - \overline{A_{ij}})(B_{ij} - \overline{B_{ij}})}{\left[\sum_{i=1}^{M_i} \sum_{j=1}^{M_j} (A_{ij} - \overline{A_{ij}})^2 \sum_{i=1}^{M_i} \sum_{j=1}^{M_j} (B_{ij} - \overline{B_{ij}})^2\right]^{1/2}} \quad (4.12)$$

where M_i and M_j are the dimensions of the IA in pixels; A_{ij} and B_{ij} are the gray scale intensity of the consecutive rectangles (IA and SA). The displacement with the highest correlation is accepted for every grid point, then the velocity vectors are calculated ($displacement/\ \delta t$). The flow chart of the algorithm is presented in **Fig. 4.19**.

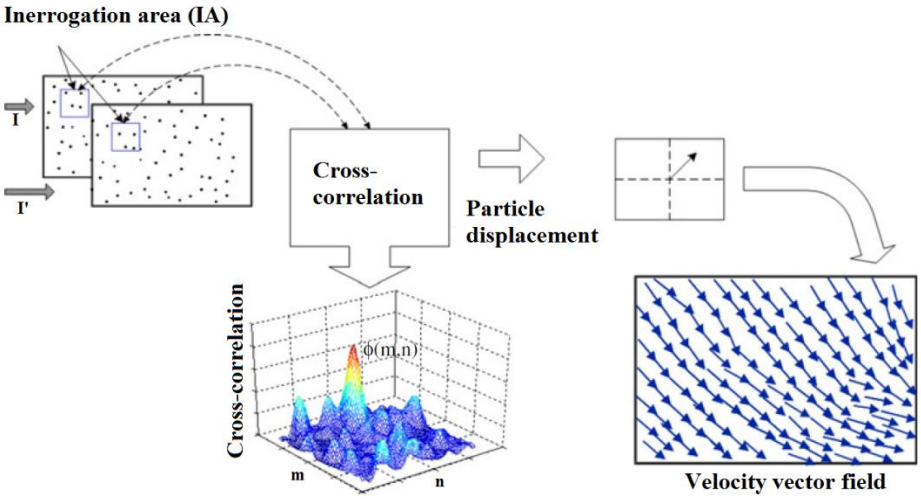

Figure 4.19 – Flow chart of the LSPIV algorithm (*Jodeau et al., 2013*)

The software offers different options to remove erroneous values from the instantaneous results. The results can be filtered with a range of accepted correlation coefficient: if the calculated displacement has a lower R than the given minimum, the result is to be removed. The other option is to set a maximal and minimal velocity value for both directions, which is an effective way to remove implausibly high velocity vectors as well.

4.5.2 Results

In order to quantitatively evaluate the dynamic characteristics of waves based on video recordings, it is necessary that the approaching waves break, so the appearing foam could be identified by the LSPIV algorithm. Two dimensional (surface) velocity vectors fields were obtained as a result of LSPIV. The result files were exported for further analysis with the visualization software, Tecplot. The velocity vector scatters were linearly interpolated to a mesh with a Tecplot macro. It is noted, that not all video files were suitable for the LSPIV analysis, because of various reasons. In some cases, the shadows of the near bank trees disturbed the method, since the projection of the moving leaves on the water surface provided traceable patterns, thus their movement was evaluated in addition to the actual movement of foam on the free surface. Also if the waves do not break at all, and only minimal foam appears as they run out to the bank, the method has nothing to identify and follow, therefore it fails. It is noted – with the consideration of the listed limitations – that the method was not applicable for all cases, only the most intense sections of the wave events were suitable for the analysis, if light conditions were suitable at all. **Fig. 4.20** presents a section of the calculated results.

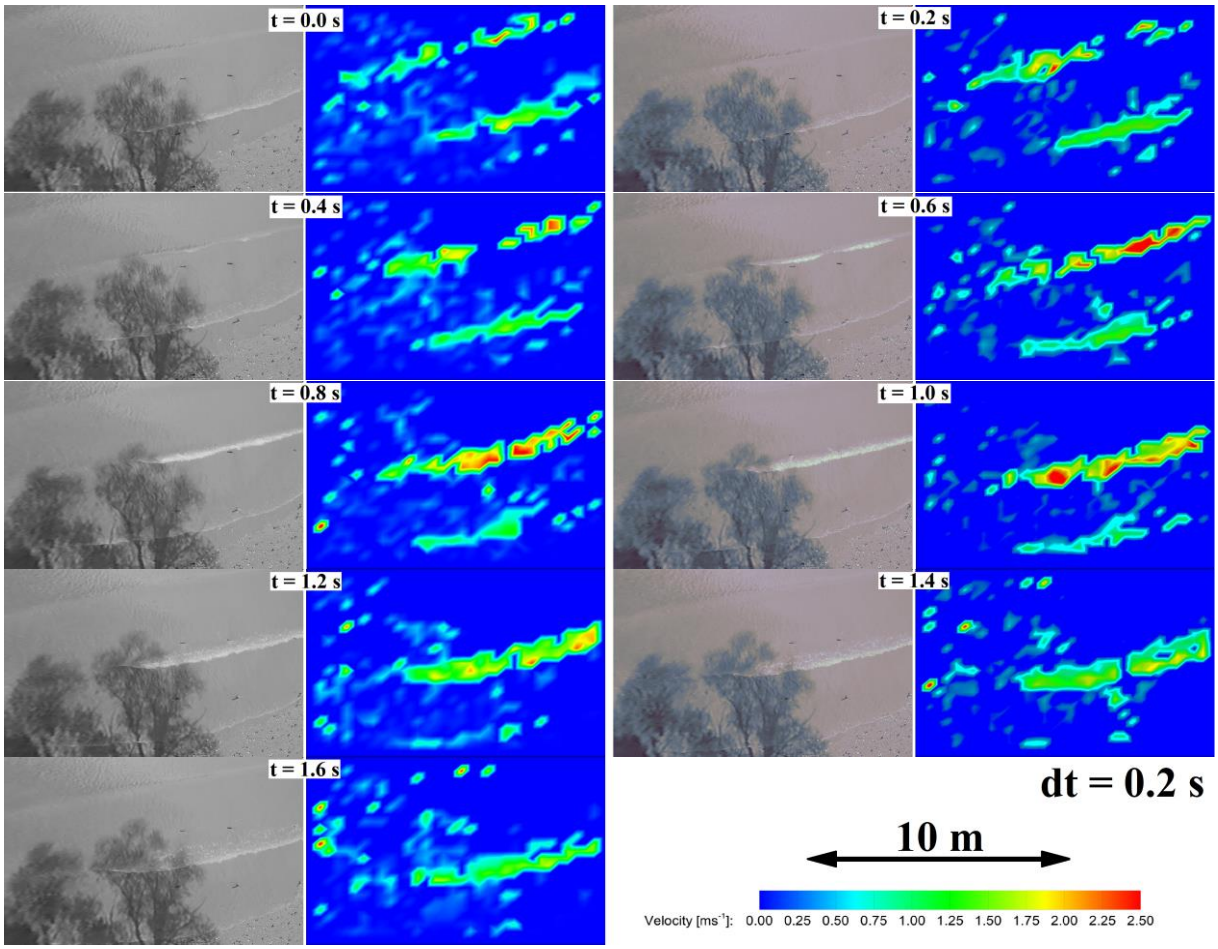

Figure 4.20– Phase speed estimated with LSPIV (14:01)

Foam appearing due to breaking waves was found to be suitable for the algorithm to identify and follow. It is noted, that results in the area of the tree shadow are more likely to be loaded with erroneous values, the velocity field is noisier there. Results presented in **Fig. 4.20** belong to the most intense section (~ t = 200 s) of the wave event induced by a hotel ship 14:01. The methods estimates wave phase speed of approximately 2 ms^{-1} which is a fair match, compared to the calculated average value for this section (1.95 ms^{-1}) presented in **Fig. 4.17**.

Masselink and Puleo, 2006 summarized the available knowledge on swash zone morphodynamics and presented methods wherewith breaking wave related erosion forces can be estimated. Rather than basing estimates for shear stress τ from velocity profile data, the typical approach relies on the quadratic stress law using the free stream velocity u, rather than the friction velocity u_* as:

$$\tau = \rho u_* |u_*| = \frac{1}{2} \rho f u |u| \tag{4.13}$$

Note, that right side of this equation was already presented in **Eq. 4.8**. Velocities calculated with LSPIV were used to present an experimental method for the estimation of shear stress

based on video records. The free flow velocity u in the equation was determined with the following assumptions:

- In the area where the wave breaking occur, the water depth is shallow enough to approach the phenomenon from a two-dimensional aspect → free flow velocity u equals the depth averaged velocity $\bar{u}$ in every point of the computational grid
- In the near-bank area, the LSPIV method estimates the propagation velocity of the approaching wavefronts, therefore, the estimated velocity is the free flow velocity related to the breaking waves on the free surface $u_{surface}$
- The depth averaged velocity $\bar{u}$ is proportional to the surface velocity $u_{surface}$ the proportionality factor is 0.85 (*Dramis et al., 2011*)

consequently:

$$u = \bar{u} = 0.85 \cdot u_{surface} \tag{4.14}$$

The use of **Eq. 4.13** presents another difficulty in terms of the appropriate value for f and much effort has gone into its estimation (*Raubenheimer et al., 2004*). Considering the highly experimental nature of the presented method, constant value of $f = 0.01$ was employed for the test calculations based on *Raubenheimer et al., 2004.*

Maximal values of surface velocities were evaluated for the test period (13.3 secs), for each point of the computational grid (~ 400 frames [13.3 s x 30fps]) (**Fig. 4.21**). Note that the orientation of the figure is the same as in **Fig. 4.20**, the waves come from the top of the frame and travel to the bottom, in the direction of the bank.

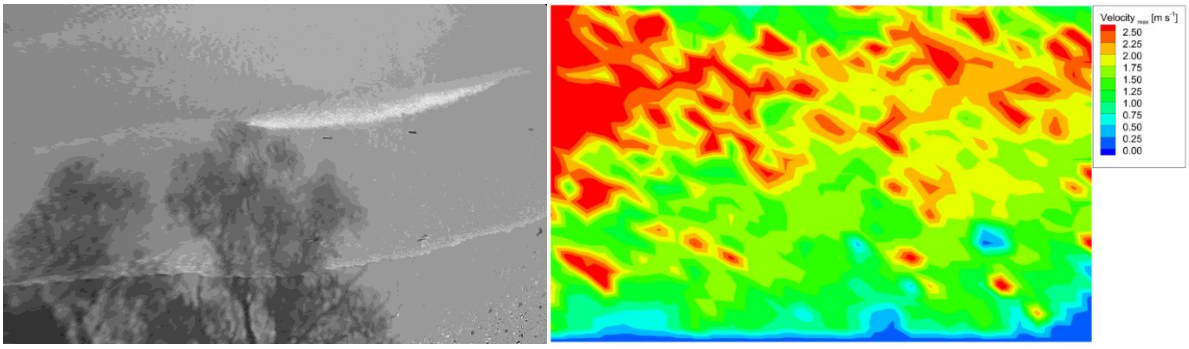

Figure 4.21 – A single moment (transformed) from the video record (left); and maximal surface velocities for the test period (13.3 secs) (right)

Note that the maximal values are lower in the bottom edge of the frame, because the wave breaking happens in the upper half, thus most of the kinetic energy is lost there. The blue colored part of the figure indicates the bank, with zero velocities.

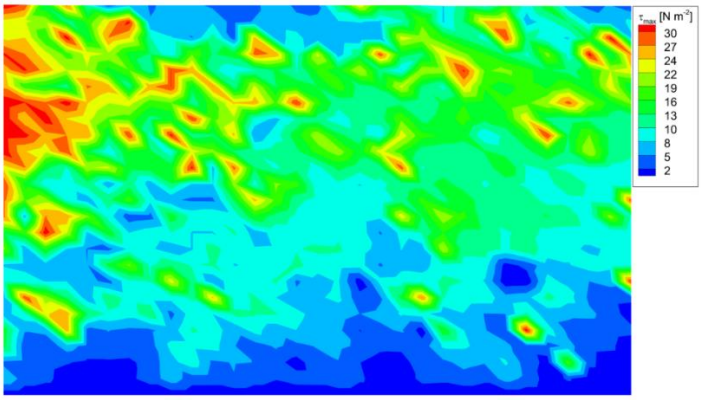

Figure 4.22 – Maximal estimated bottom shear stress for the test period (13.3 secs)

However, it is noted, that significant simplifications were applied in order to estimate erosion forces from surface velocity vector fields, it is still stated, that the employment of this method has relevance in applied hydraulic engineering, since bank erosion is a very common problem in riverine, lacustrine and marine conditions as well. Furthermore, these shear forces may also affect the ecosystem of the littoral zone, which is also a significant problem, which cannot be ignored (WFD). Not only the relationship between free flow velocities and surface velocities has to be clarified, but the whole interaction between the fluid and the substrate requires further investigations. It has to be noted, that such methods have to deal with the inconvenience caused by the fact, that there is no widely accepted method available for the direct estimation of bottom shear stress, therefore, the validation of these methods is quite circumstantial.

5 Numerical modeling

This chapter covers the basic principles of computational fluid dynamics (CFD) in general, along with the introduction of REEF3D, the CFD model used in present study. The employed numerical setups (geometry, computational mesh, boundary conditions) and the results will also be presented.

5.1 The employed CFD model: REEF3D

REEF3D is a fairly new open-source CFD model, developed at the Department of Civil and Transport Engineering of the NTNU by Hans Bihs. The software comes without graphical user interface (GUI), the different functions and parameters has to be given in a file called the 'control file'. For each function of the solver, there is a codename consists of a letter and a number, followed by another number which sets the value of the function e.g. the 'D 10' function is to select the convection discretization scheme for the momentum equations and with 'D 10 1' the first order upwind scheme will be employed. The features and functions provided by REEF3D are listed and detailed in the user manual of the software (*Bihs, 2015a*).

REEF3D uses finite difference method for the numerical discretization of the governing equations. The free surface is determined with the Level Set Method (LSM) (*Osher and Sethian, 1988*), which grants high accuracy, however the Volume of Fluids (VOF) method (*Hirt and Nichols, 1981*) is built in the code as well. There are several turbulence models included in the code, starting from the widely used variations of Reynolds-Averaged Simulations (RAS) and Large Eddy Simulation (LES) as well. The software prints the result files in binary format, compatible with ParaView, a freely available open-source post-processing visualization software.

The model only works with a Cartesian computational grid. On one hand, this makes the implementation of the numerical algorithms straightforward, but on the other hand, this kind of grid is not very flexible due to its well defined structure. Cartesian grids cannot be wrapped around complex geometry, which can easily become a problem, when an irregular structure is placed in the fluid domain or when working with natural channels. The ghost cell immersed boundary method (GCIBM) (*Berthelsen and Faltinsen, 2008*) is employed to overcome this problem. Values from the fluid region are extrapolated into the solid region and these cells are called 'ghost cells'. The value of these cells are computed along an orthogonal line across the boundary (**Figure 5.1**).

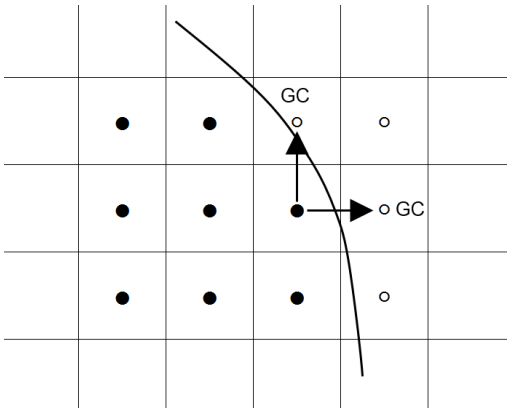

Figure 5.1 – Ghost Cell Immersed Boundary

A software called DIVEMesh is responsible for mesh generation for REEF3D. DIVEMesh (*Bihs, 2015b*) is also being developed by Hans Bihs specifically to create computational grids for REEF3D.

5.2 Numerical and mathematical background

In this section, the numerical and mathematical background of REEF3D will be briefly presented. For more detailed information, see *Bihs, 2011*.

The employed CFD model solves the RANS equations (**Eq. 5.2**) with the continuity equations (**Eq. 5.1**) for incompressible flow using finite difference method. The idea behind the equations is to decompose the instantaneous velocity vectors into its time-averaged and fluctuating components (*Reynolds, 1895*). The averaged component is directly used in the equations and the effect of the fluctuating component is approximated by the introduction of eddy viscosity to the equations:

$$\frac{\partial U_i}{\partial x_i} = 0 \tag{5.1}$$

$$\frac{\partial U_i}{\partial t} + U_j \frac{\partial U_i}{\partial x_j} = -\frac{1}{\rho}\frac{\partial P}{\partial x_i} + \frac{\partial}{\partial x_j}\left[(\nu + \nu_t)\left(\frac{\partial U_i}{\partial x_j} + \frac{\partial U_j}{\partial x_i}\right)\right] + g_i \tag{5.2}$$

where U is the velocity averaged over time; ρ is the fluid density; P is the pressure; ν is kinematic viscosity; ν_t is the eddy viscosity and g is the acceleration due to gravity. The convection term of the RANS equations is discretized with the Weighted Essentially Non-Oscillatory (WENO) scheme (*Jiang and Shu, 1996*). Here, a discretization stencil consists of three substencils, which are weighted according to the local smoothness of the discretized function. The scheme achieves a minimum of 3rd-order accuracy for discontinuous solutions, up to 5th-order accuracy for a smooth solution and provides with robust numerical stability. Time discretization of the momentum equations is achieved with a third-order accurate total variation diminishing (TVD) Runge-Kutta scheme (*Shu and Osher, 1988*). The pressure term

is solved with the projection method (*Chorin, 1968*) and the BiCGStab algorithm (*van der Vorst, 1992*) with Jacobi scaling preconditioning solves the Poisson equation for the pressure. The RANS equations are closed with the two-equation k-ω turbulence model (*Wilcox, 1994*):

$$\frac{\partial k}{\partial t} + U_j \frac{\partial k}{\partial x_j} = \frac{\partial}{\partial x_j}\left[\left(\nu + \frac{\nu_t}{\sigma_k}\right)\frac{\partial k}{\partial x_j}\right] + 2\nu_t|S|^2 - k\omega \tag{5.3}$$

$$\frac{\partial \omega}{\partial t} + U_j \frac{\partial \omega}{\partial x_j} = \frac{\partial}{\partial x_j}\left[\left(\nu + \frac{\nu_t}{\sigma_\omega}\right)\frac{\partial \omega}{\partial x_j}\right] + 2c_\mu c_{\omega 1}|S|^2 - c_{\omega 2}\omega^2 \tag{5.4}$$

where ω is the specific turbulent dissipation, k is the turbulent kinetic energy and coefficient $c_\mu = 0.09$, $c_{\omega 1} = 5/9$, $c_{\omega 2} = 5/6$ and $\sigma_k = \sigma_\omega = 2$. The term $|S|^2$ can be written as:

$$S_{ij} = \frac{1}{2}\left(\frac{\partial U_i}{\partial x_j} + \frac{\partial U_j}{\partial x_i}\right) \tag{5.5}$$

The main feature of breaking waves is the complex motion of the free surface. The model employs the level set method (*Osher and Sethian, 1988*) to capture the free surface between the two phases: air and water. The method uses a signed function, called to level set function to capture the free surface. The property of this function $\phi(\vec{x}, t)$ is that its value gives zero on the free surface. In every point of the computational domain, the level set function gives the closest distance to the interface and the phases are distinguished by the sign, as following:

$$\phi(\vec{x}, t) = \begin{cases} > 0, & if\ \vec{x}\ \epsilon\ phase\ 1 \\ = 0, & if\ \vec{x}\ \epsilon\ \Gamma \\ < 0, & if\ \vec{x}\ \epsilon\ phase\ 2 \end{cases} \tag{5.6}$$

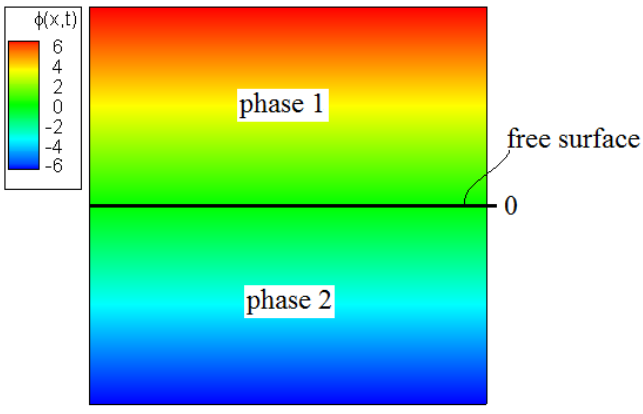

Figure 5.2 – The level set function

The interface moves with the fluid particles and its movement can be described with the convection of the level set function:

$$\frac{\partial \phi}{\partial t} + U_j \frac{\partial \phi}{\partial x_j} = 0 \tag{5.7}$$

The assumption of incompressibility and immiscibility of the fluids cause a jump in the values of the parameters at the interface, which may lead to numerical stability problems. This is avoided by smoothing the material properties in the region around the interface with a regularized Heaviside function $H(\phi)$. This region is 2ϵ thick, with ϵ being proportional to the grid spacing Δx. In the present study it was chosen to be $\epsilon = 1.6\,\Delta x$. The density (ρ) and the viscosity (ν) can be written as:

$$\begin{aligned} \rho(\phi) &= \rho_1 H(\phi) + \rho_2\big(1 - H(\phi)\big) \\ \nu(\phi) &= \nu_1 H(\phi) + \nu_2\big(1 - H(\phi)\big) \end{aligned} \tag{5.8}$$

and the regularized Heaviside function:

$$H(\phi) = \begin{cases} 0, & if\ \phi < -\epsilon \\ ½\Big(1 + \frac{\phi}{\epsilon} + \frac{1}{\pi}\sin\big(\frac{\pi\phi}{\epsilon}\big)\Big), & if\ |\phi| \le \epsilon \\ 1, & if\ \phi > \epsilon \end{cases} \tag{5.9}$$

5.3 Numerical setups

5.3.1 2D model

Numerical simulations had been conducted to present that the basic fluid mechanical characteristics of ship induced waves can be reproduced in the littoral zone via CFD in significantly simplified geometrical and hydraulic conditions. A validated model for example, might provide with the opportunity to fulfill the impact analysis of the planned gravel bed, which would hopefully reduce the negative effects of ship induced waves in the littoral zone of the studied river reach, thus would provide a safer and more stable environment for local macroinvertebrates and juvenile fish.

Considering the extremely high computational demands of the model, the validation was fulfilled on a two-dimensional slice model with a depth of 1 cell. It is noted, that the simulations were executed under supercomputing environment, because of the high demands of the solver.

The bathymetry was built based on the GPS measurements, however, because of the limited mesh generating functions of DIVEMesh, the geometry had to be built from three right-angled tringles (**Fig. 5.3**) with a uniform grid size of $dx = 1\ cm$.

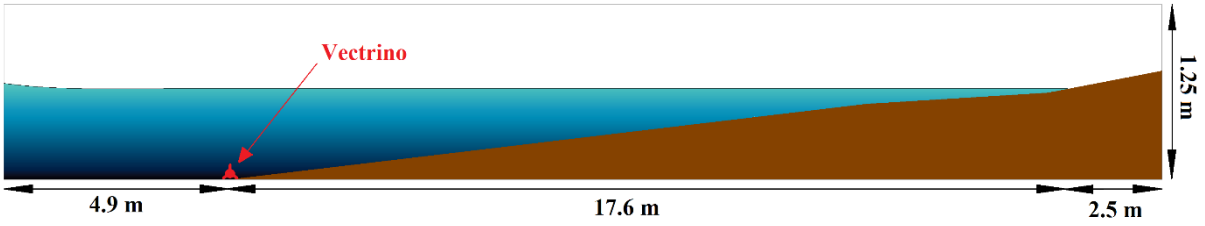

Figure 5.3 – 2D Computational domain and its dimensions with the initial condition (the figure is vertically distorted (3x))

The still water level for the simulations was also taken from the GPS measurements, and the roughness height of the bottom boundary (k_s) was derived from the grain size distribution of the substrate sample (**Fig. 5.4**):

$$k_s = 3 \cdot d_{90} \tag{5.10}$$

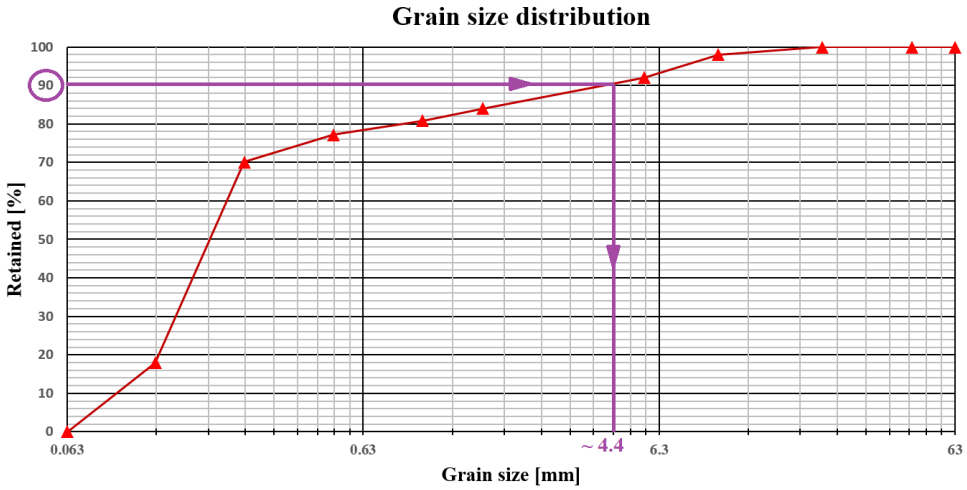

Figure 5.4 – Grain size distribution of the substrate

REEF3D requires two wave theory related parameters for configuring boundary conditions (pressure and velocity profiles) at the inflow boundary: amplitude (A) and wavelength (L) or amplitude and wave period (T). In present study wave amplitude and wave period was used which had been derived from the pressure measurements obtained by the Aquadopp device. One of the most intense wave event section was selected for numerical modeling, with an amplitude of $A = 4\,cm$ and period of $T = 2.8\,s$. The waves were generated according to linear wave theory. Measured and calculated near-bed velocity series were compared to verify the numerical results, since this is one of the most relevant parameter from the ecohydraulic aspect (**Fig. 5.5**).

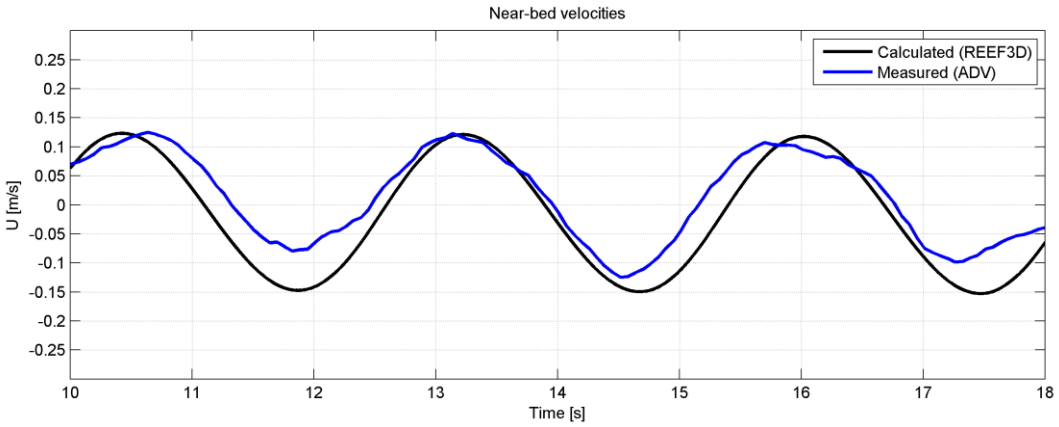

Figure 5.5 – Measured and calculated near-bed velocity series (model validation)

Results confirm the applicability of the model for the investigation of ship induced waves, however, it is noted that the perfect reproduction of the field data cannot be expected, because of the high complexity of the flow and the natural environment as well. Nevertheless, these numerical investigations could mean further steps towards understanding the main features and characteristics of ship induced waves in riverine conditions.

Although, the numerical results provided by the fine grid ($dx = 1.0\ cm$) showed good match with the measurements, the sensitivity analysis of the cell size had to be conducted, since 3D simulations in such fine resolution would have took months to finish, even under supercomputing environment. The task was to find an optimal cell size which provides accurate and plausible results and reasonable computational demands at the same time.

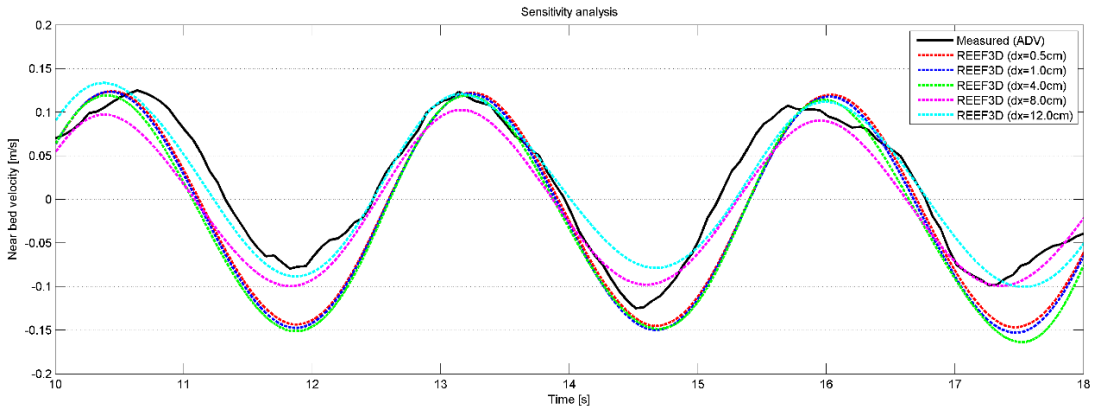

Figure 5.6 – Sensitivity analysis for grid size

Fig 5.6 presents the result of the sensitivity analysis. Almost perfect overlap is observed between the 0.5, 1.0 and 4.0 cm grids, which shows that the reference simulation ($dx = 1.0\ cm$) could had been conducted on even four times courser grid, and still would have provided the same quality result for this comparison. The employment of courser and coarser girds, however, resulted in higher and higher deviations from the previously observed ones. It

is noted, that in some specific sections, the courser meshes provided even better match with the measurements than the high resolution ones, which can be explained by the irregularity of the real waves.

Though, the finest grid ($dx = 5\ mm$) did not provide more accurate, nor detailed results compared to the reference resolution in the comparison of near-bed velocities 15 m from the bank, this does not mean, that the whole fluid flow problem is not resolved more accurately in general. The closer the waves get to bank, the more it requires the finer grid resolution for the proper and accurate reproduction of the appearing real life phenomena, such as breaking waves. Wave height is limited by both depth and wavelength. For a given water depth and wave period, there is a maximum height limit above which the wave becomes unstable and breaks. This upper limit of wave height, called breaking wave height, is a function of the wavelength in deep water. In shallow and transitional water, it is a function of both depth and wavelength. Wave breaking is a complex phenomenon and it is one of the areas in wave mechanics that has been investigated extensively both experimentally and numerically (*USACE, 2002*).

There are four basic types of breaking water waves: spilling, plunging, collapsing and surging (**Fig. 5.7**).

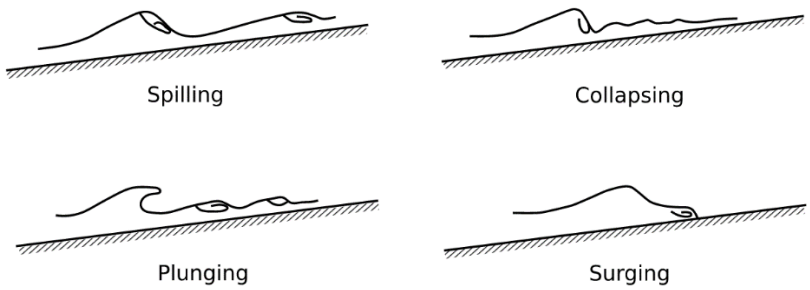

Figure 5.7 – Breaking wave types (*FHWA, 2008*)

The type of wave breaking is determined by the Iribarren number, which is a function of bank slope and wave steepness:

$$\xi = \frac{\tan\alpha}{\sqrt{H/L_0}} \tag{5.11}$$

where $\tan\alpha$ is the bank slope, H is the wave height and L_0 is the wave length at deep water.

The categorization based on the Iribarren number is the following:

$$\begin{aligned} &spilling && if && \xi < 0.5 \\ &plunging && if && 0.5 < \xi < 3.0 \end{aligned}$$

$$collapsing \quad if \quad \xi = 3.0$$
$$surging \quad if \quad \xi > 3.0$$

During the field measurements breaking waves were observed, in fact the appearing foam made it possible to investigate the phenomenon with LSPIV. Therefore, it is expected that the numerical results also reproduce these characteristics. Based on the criteria above which is a function of wave parameters and geometry, plunging breakers are expected for present case. **Fig. 5.8** presented the breaking (plunging) of a wave for the tested case modeled via REEF3D.

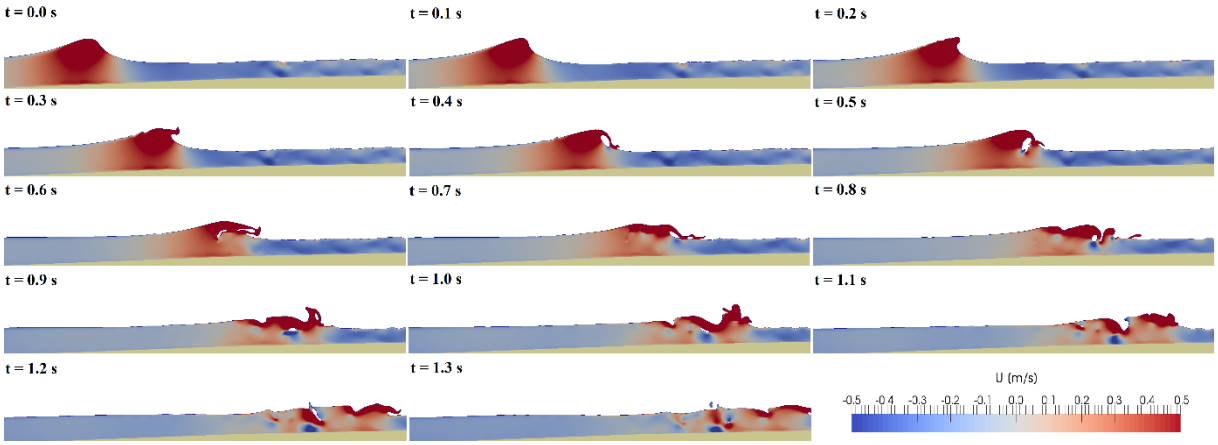

Fig. 5.8 – Breaking of approaching waves modeled with REEF3D ($\Delta t = 0.1\ s$)

The numerical results match the characteristics of plunging breakers presented in **Fig. 5.7**. The water phase has been colored based on the horizontal velocity component, red is for the direction towards the bank, blue is towards the thalweg. These results emphasize the relevance of the Level Set Method in the numerical modeling of multiphase flows.

It is noted, that coarser grids are unable to reproduce wave breaking, therefore the bank erosion derived directly from breaking waves, could not be calculated properly in lower resolutions.

5.3.2 3D model

Although the $dx = 12.0\ cm$ grid showed the highest deviation from the reference velocity series in the 2D sensitivity analysis, it was still found to be the most appropriate choice for the 3D simulations (~ 4.5 million cells). The accuracy of the simulations had to be sacrificed in order to preserve reasonable computing times.

The 2D model was not only expended by its depth to create a reference geometry for the 3D simulations, but the near-bank area was deepened and steeper slopes were applied as well. This morphological modification was planned along with the artificial gravel bar. Present

study only aims to numerically investigate the hydrodynamic and ecohydraulic effects of the gravel bar, therefore it was only compared with the similarly modified reference condition.

It is noted, that because of the limited meshing options provided by DIVEMesh, the geometry of the gravel bar is not even remotely similar to natural formations, however the original idea was to be so (Chapter 2.1). Considering this, and the fact that the used computational mesh resolution is not considered to be optimal either, it is emphasized that the following numerical tests are considered to be only qualitative investigations.

The following figures present the geometries and dimensions of the 3D domains.

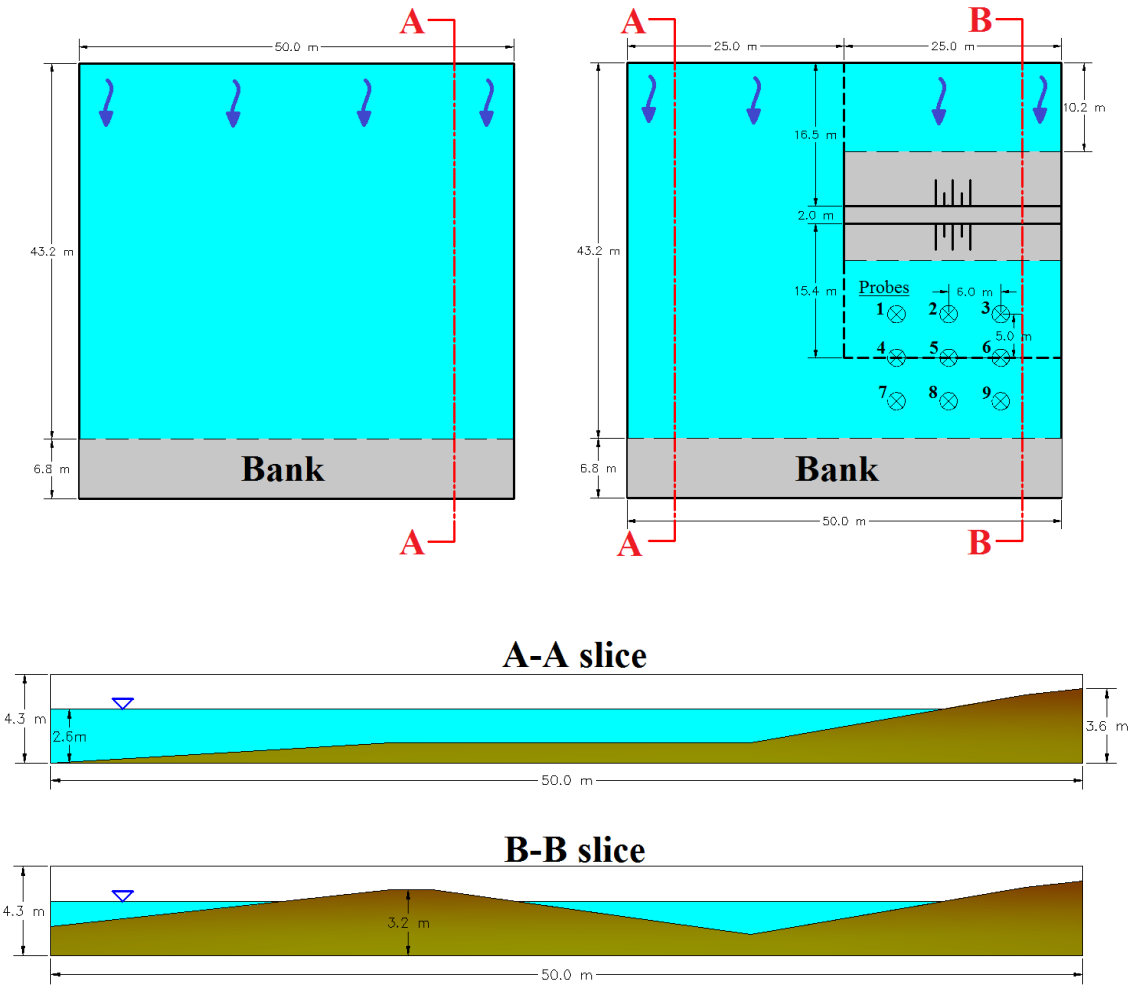

Figure 5.9 – Computational domain for the reference (left) and the modified (right) state, at h_0=260cm with the location of the probes.

Three different water level conditions were numerically investigated with the same wave boundary conditions as in the 2D simulations ($A = 4\ cm$ and $T = 2.8\ s$). The three employed water levels – measured at the start of the domain – were:

- $h_{0,1} = 2.0\ m$ – equivalent to the low water condition where the field measurement campaign was held, therefore to the 2D initial setup as well

- $h_{0,2} = 2.6\ m$ – half way between the low water condition and the top of the bar
- $h_{0,3} = 3.2\ m$ – still water level is at the level of the bar crest

It is noted that during floods even higher water levels can be expected at the study sight, and that the hydraulic phenomena appearing when the bar is fully submerged would be interesting and instructive to investigate, these situations were left out. The reason for this, is that in higher water level conditions, the groins become submerged as well, therefore the whole hydraulic character of the backwater changes, where the assumption of negligible background current becomes impermissible.

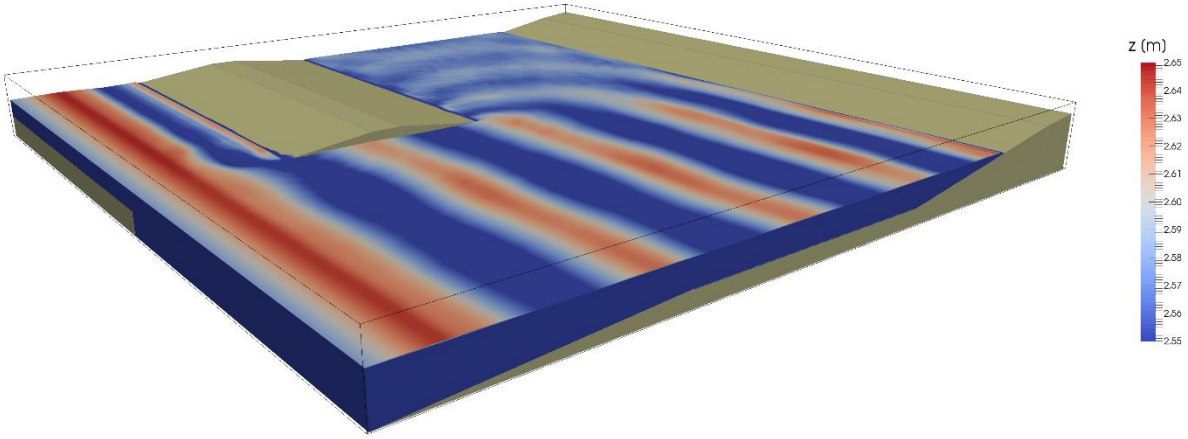

Figure 5.10 – 3D numerical result ($h_{0,2}$), the water volume is colored based on elevation

The 3D model provided with detailed complex flow characteristics. However, **Fig. 5.10** presents the numerical results (colored based on elevation) for only a single timestep, it provides with valuable information. The figure is a decent object-lesson for wave diffraction, which occur when a wave encounters an obstacle in the water. The wave height reducing effect of the gravel bar also appears, which is expected to imply the reduction of bottom shear stress in the shaded area as well (the effect of shorter waves is damped in the direction of the bed). However, the employment of the $dx = 12\ cm$ cell sized grid was found not to be the perfect choice during the 2D sensitivity analysis, these result point out, that this course resolution is also able to describe detailed wave related flow features.

In addition to the three dimensional parameter fields, data had been printed out for nine point probes in order to make it easier to compare the results. The probes were located right above the river bed, behind the gravel bar and were also situated in the very same position in the reference geometry, in order to make comparisons possible. The location of the probes is presented in **Fig 5.9**.

Bottom shear stress is the most relevant flow related parameter from the ecological (ecohydraulic) aspect, hence was used as an indicator for the numerical comparisons. The lower the bottom shear stress is, the less fish eggs and macroinvertebrates are to be detached from the river substrate. Since the idea behind the building of the presented gravel bar is to provide a safer and more stable habitat for these creatures, lower bottom shear stress values are expected compared to the reference state.

Previous studies reported that the numerical treatment of morphological changes generated by wave induced bottom shear stress is possible (*Afzal et al., 2015*), where the bottom shear stress is determined as (*Zeng et al., 2005*):

$$\tau = -\rho(\nu_t + \nu)\frac{\partial U}{\partial z} \tag{5.12}$$

Eq. 5.12 was used to calculate bottom shear stress from the probes' time series.

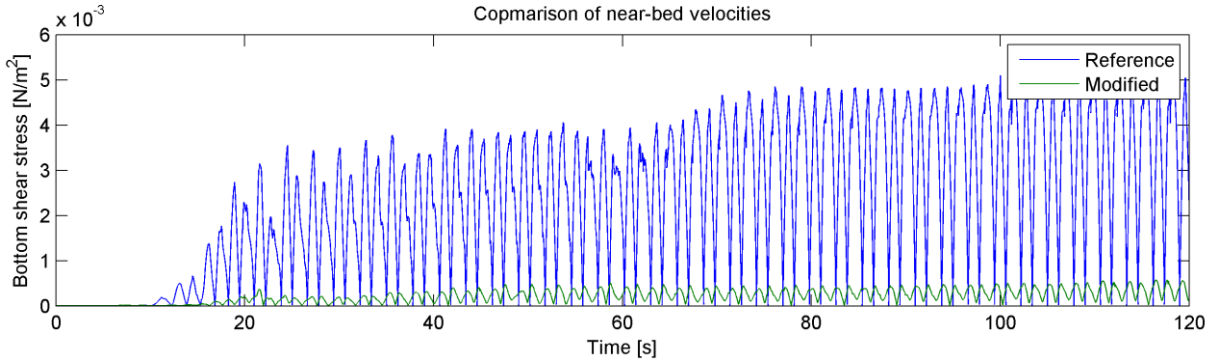

Figure 5.11 – Comparison of the calculated bottom shear stress ($h_{0,2}, probe\ 7$)

Bottom shear stress reduction of almost a magnitude is observed on **Fig. 5.11**. Previous studies reported that bottom shear stress generated by ship is rapidly increasing as the waves transform while getting closer and closer to the bank (*Fleit 2014a, Fleit 2015*). The probe is in the shade of the gravel bar, where the waves cannot transform in the regular way, wave diffraction occurs because of the obstacle and the waves die down, consequently bottom shear stress is reduced significantly as well. In order the preserve space and to enhance intelligibility, the rest of the results will not be presented as time series, but as surfaces. Maximal values of bottom shear stress will be presented and compared in 3D plots, for the three water level conditions. Note that the 9 points used for plotting the 3D figures are the ones presented on **Fig. 5.9**. It is also noted, that the changes between the sampled points are probably not linear, the interpolation of the presented grids are only aim to help the apprehension of the phenomenon. On the left side of **Fig. 5.12** the geometry of the 3D model is presented. The red ellipse marks the area behind the bar, from where the bottom shear stress

values were queried, and the axes are also presented to help the apprehension of the following figures (the orientation of the figures is also the same). Note that the bottom shear stress values generally decreased due to the gravel bar, therefore the upper surfaces always belong to the reference state.

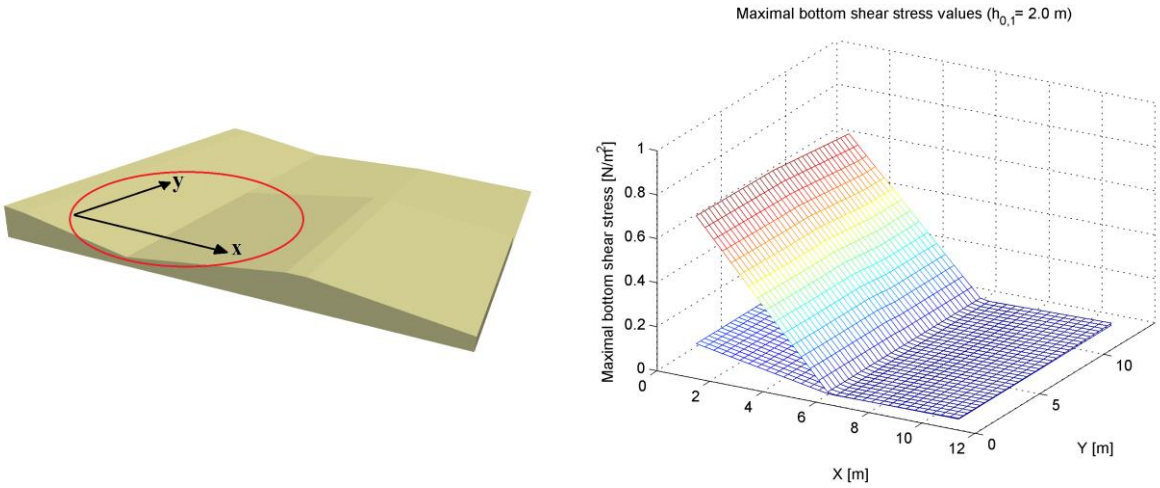

Figure 5.12 – Modified 3D geometry (left) and maximal bottom shear stress values for $h_{0,1} = 2.0\ m$ (right)

Note that the range of the vertical axis (τ) is different in **Fig. 5.12** and **Fig. 5.13**.

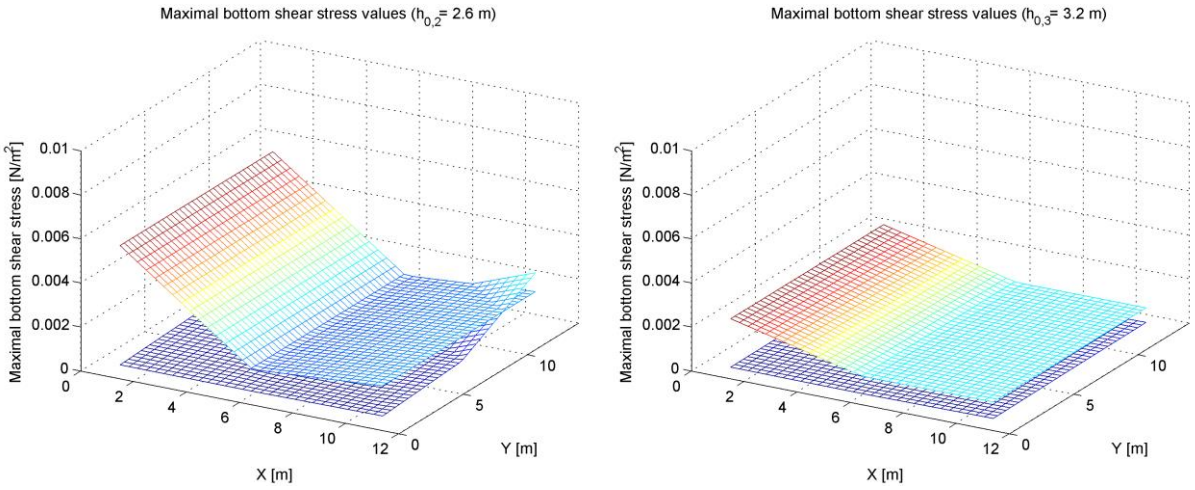

Figure 5.13 – Maximal bottom shear stress values for $h_{0,2} = 2.6\ m$ (left) and $h_{0,3} = 3.2\ m$ (right)

The case with the lowest still water level shows two magnitudes higher bottom shear stress values near the bank, compared to the other ones, which is explained by the fact, that the probes were in the wave breaking zone, and however, the waves did not break in such course resolutions, the near-bed velocities still grew high enough to result such high shear forces. It is also noted, that the modification removes these salient values, wave breaking would probably not occur behind the bar in real life. On the left side of **Fig. 5.13** it is observed, that bottom shear stress gets higher in the corner of the gravel bar in the modified case. This is

probably a consequence of wave diffraction (**Fig. 5.10**), the emerging transversal current induces increased shear forces compared to the reference state, however, this effect dies down as it gets further from the edge of the structure. This effect also probably comes from the sharp-edged shaping of the bars, which comes from the mesh generating limitations.

Apart from these irregularities, in general it can be stated, that the gravel bar does reduce wave related bottom shear stress in its shaded area, furthermore, the higher the still water level gets, the lower the shear forces will become in the littoral zone, for waves of same characteristics. However, it has to be pointed out, that the characteristics of ship induced waves might change significantly in different water level conditions. In order to explore these relations in detail, further field and computational investigations are required.

6 Ecohydraulic sample application

Gabel, 2012 investigated the effect of waves on macroinvertebrates in different type of habitats (coarse woody debris, reeds, tree roots, sand and stones). Experiments were conducted in laboratory conditions with an experimental wave tank and in real life lacustrine conditions as well, with motorboat generated waves. The idea behind the experiments was that the different macro scale creatures differ considerably in body shape, locomotion behavior and attachment strategies, all of which influence their sensitivity to wave impact. On the other hand, different habitats reduce the amount kinetic energy on the bed, hence bottom shear stress as well, which is responsible for detachment of individuals. The five different habitats were formed in trays and specified amount of macroinvertebrates (n=20) were placed on the trays from each species. They were held in still water at the beginning in order to facilitate their attachment to the substrate.

During the wave events, maximal bottom shear stress was estimated with the Jonsson-method, based on ADV measurements, and the number of detached individuals were also recorded, so the relation between these parameters could further be analyzed with statistical methods.

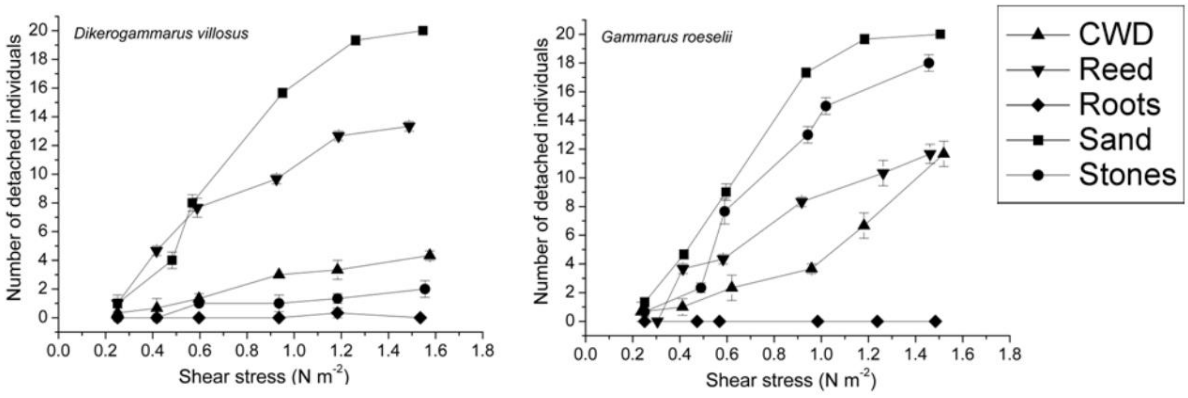

Figure 6.1 – Number of detached individuals as a function of wave generated bottom shear stress (*Gabel, 2012*)

If the relationships between detaching forces and the detachment rates of different species are known, the ecological effects of ship induce waves can be quantified. Maximal bottom shear stress values were estimated in the location of the ADV device (15 m from bank) in section 4.4. With the presumption that the *Dikerogammarus villosus* might be present in the study site, and that the relationship presented in **Fig. 6.1** are applicable in a Hungarian section of the Danube, the proportion of detached individuals can be estimated based on the calculated shear forces. As it was previously noted, the substrate material was mostly sand in the investigated near-bank area, therefore, that graph was used for the following sample application.

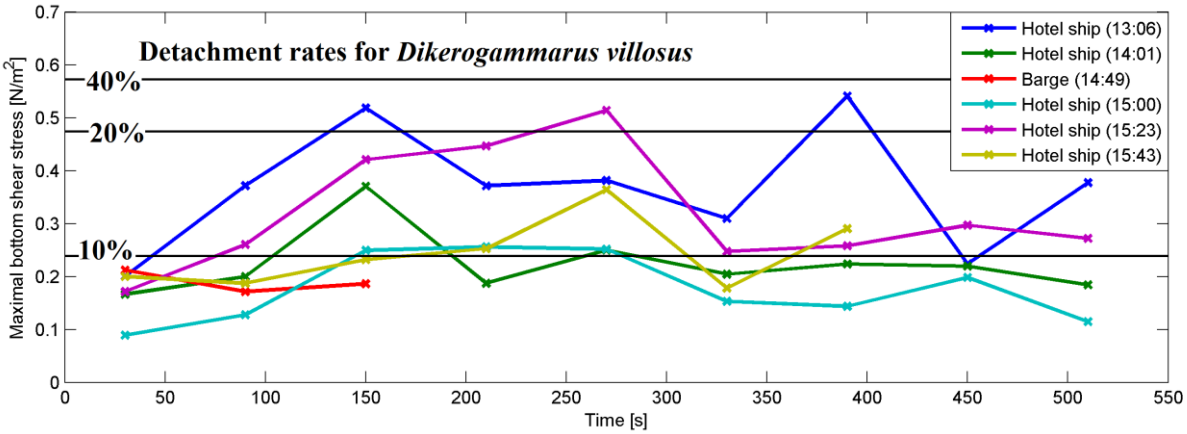

Figure 6.2 – Temporal distribution of maximal bottom shear stress for different ships (**Fig. 4.18**), completed with the detachment rates of *Dikerogammarus villosus* (**Fig. 6.1**)

It is observed, that shear forces generated by ship induced waves in ~15 m distance from the bank would be able to detach approximately 10-20 % of the population of the chosen macroinvertebrate species. Previous studies reported that wave related shear forces increase rapidly in the direction of the bank, which leads to higher detachment rates as well, even up to 100 % (*Fleit, 2014a*). This is further supported by results provided by the experimental, LSPIV-based, wave breaking related shear force estimation method, where the shear forces increased to up to 15-20 N m^{-2} which is significantly above the values for the total (100 %) detachment of the investigated species.

It is once again noted, that these results are only aim to present, that there are methods already available for estimating the ecological effect of ship induced waves from the aspect of macroinvertebrate detachments. The relevance of joint measurements with biologist is also emphasized, these methods need further developments, which requires the cooperation of multiple disciplines.

7 Summary

Comprehensive analysis of ship induced waves was completed in a Hungarian section of the Danube. The study site was a backwater between two groins, and by the way was the same as in previous year's study (*Fleit, 2014a*).

Both the field measurements and the data processing/analyzing methods were significantly developed based on previous year experiences. Near-bed velocity times series were obtained by an ADV device, and a new velocity profiler (Aquadopp) was also applied, which was equipped with a pressure gauge as well. The field measurements were complemented with two- and three-dimensional numerical modeling as well, which provided with the opportunity to complete the impact analysis of a planned artificial gravel bar, which would provide a safer and more stable habitat to the local aquatic fauna.

Near-bed velocity time series were quality checked to eliminate erroneous measurements before further analysis. Background velocities and wave related flow velocities were decomposed, the time series were detrended. Principal component analysis was carried out on the detrended data, in order to determine the principal direction of ship induced waves, and to inspect their relationship with the ships' direction of travel.

The spectral density of the near-bed velocities was calculated with discrete Fourier transformation. These investigations unfolded the fact that ship induced wave events basically consists of two significant wave-types: relatively high frequency waves (T = 3-4 sec) which can be easily observed from the bank after the passing of a ship and low frequency waves (T = 60-90 sec) which could also be detected on the video recordings as a movement of the touchline.

The velocity profiler (Aquadopp) was deployed for the very first time during the field measurements, the main aim of its application was to test its capabilities and to meet its limitations. However, the high resolution velocity profile measurements pointed out the three-dimensional nature of the combined effect of ship induced flows and the background flow between the groins. The results also emphasized the relevance of three-dimensional numerical modeling for the investigation of ship induced wave related flow phenomena.

The spectral density of the pressure measurements was calculated and compensated in order to return the spectral density of the surface elevations, which carries the potential to evaluate important, representative wave parameters (significant wave height, wave period, wave length). Time series were decomposed into 60 seconds long sections, so the temporal distribution of these parameters could be inspected.

These scientifically grounded results provided with the opportunity to conduct more accurate bottom shear stress estimations, compared to previous year's study. The correct estimation of this parameter is vital, since this flow related parameter is often associated with ecological effects, therefore it could be a common ground between hydraulic engineers and ecologists, when doing inter-disciplinary research.

All data processing and analysis up to this point was completed with self-developed MATLAB scripts.

Large scale particle image velocimetry was also employed to quantify the propagation speed of breaking waves near the bank. The method was found to be applicable for tracing and following the foam appearing due to wave breaking. An experimental method had been elaborated to estimate shear forces related to wave breaking, which is primarily responsible for bank erosion, therefore is an important and relevant research topic not only in riverine, but in lacustrine and marine conditions as well. However, the first results were found to be plausible, it is clearly pointed out that the method contains several significant simplifications, therefore the numbers should not be accepted unconditionally.

A two-dimensional model was created to prove that ship induced waves can be numerically treated with the appropriate computational tool (REEF3D). Sensitivity analysis was conducted to find a reasonable grid resolution for three-dimensional modeling, whose computational demands are extremely high, in fact, all simulations were run under supercomputing environment. Due to the advanced free surface treatment (level set method) of REEF3D, a fine resolution model also carries the potential to numerically reproduce breaking waves, which are primarily responsible for the previously mentioned bank erosion, however, these detailed investigations in this topic, were not part of present study.

A three-dimensional model was built with coarser resolution, in order to complete the impact analysis of the planned artificial gravel bar. Despite the relatively big cell sizes, the model provided detailed results, even the effect of wave diffraction was observable on the results. The model confirmed the conjecture about the beneficial effects of the bar: wave heights and near-bed velocities decreased due to the structure, which resulted in lower bottom shear stress values as well. However, both the geometry and the boundary conditions were significantly simplified compared to real life, it is still stated that these models might become a useful part of the hydraulic engineering toolbar, when supporting habitat based river trainings.

In order to emphasize the relevance of the presented investigations, and to point out the necessity of joint, interdisciplinary research in ecohydraulics, a sample application was presented, where a flow related parameter (bed shear stress) was connected to an ecological

parameter (ratio of detached individuals), in order to estimate the changes in the population of a macroinvertebrate creature, due to ship induced waves.

8 Conclusions and outlook

The hydraulic effects of ship induced waves in the littoral zone of the Danube River were explored by means of field and computational methods. Various different field instruments were deployed and used during the measuring campaign, and the gathered data was processed with up-to-date, novel analyzing methods.

A novel and promising 3D CFD model was thoroughly tested and applied with state of art free surface calculation feature, which was found to be suitable for studying the wave propagation towards the river banks and the deformation and breaking of the waves.

The erosion effects of ship induced waves were found to be quantifiable close to the bank (and showed significant increase of bottom shear stress due to waves). It was also found, that a more intense form of erosion (due to breaking waves) is also describable with the numerical model. However, due the complex nature of the typically two-phase phenomenon of the breaking waves and the exact quantification of the local shear stress requires further investigations.

It is hypothesized that there are strong relations between different ship related parameters (speed, shape, load, etc.) and the characteristics of the wave systems they induce, however, these connections could not have been revealed yet, in absence of these ship related data.

One of the major advantages of the CFD modelling is that we are able to quantify the effects of planned manmade structures on the hydrodynamic and morphodynamic conditions of the river bank. Further development of the model could also lead to the direct simulation of moving objects (ships) in the water volume with the six degree of freedom method (6DOF), but this is rather a topic of a prospective PhD thesis. A detailed description of ship dynamics in the numerical model calls for a strong collaboration with ship engineers.

The results quite clearly showed, that further field measurements are vital in order to improve the introduced methods and widen our knowledge on the hydrodynamic effects of ship induced waves. Measurements at different water regimes would also provide the possibility to validate the numerical model for different conditions, therefore its applicability for various conditions would be scientifically grounded. The presented method for the estimation of bed shear stress based on large scale particle image velocimetry is in an initial phase, its proper adaptation also requires further investigations.

The relevance of joint measurements with ecologists is also emphasized, as clear connections between hydraulic and biological parameters are required in order to properly treat the eco-hydraulic aspect of ship induced waves. Such knowledge could be implemented directly in

CFD models, therefore the ecological impact analysis of a wave protection structure could be quantified.

Long-term statistical analysis of the passing frequency of different ships with different parameters on a specific river reach could mean the first step towards the establishment of duration curves to describe the impacts of different types of ships in the littoral zone.

The above described points well demonstrate that this study can be a strong base and starting point for a novel interdisciplinary research among river engineers, ship engineers and ecologist as we provided a complex theoretical, experimental and numerical analysis to describe the influence of ship induced waves.

Bibliography

1. Afzal M. S., Bihs H., Kamath A., Arntsen Ø. A. (2015): Three-Dimensional Numerical Modeling of Pier Scour under Current and Waves Using Level-Set methods. Journal of Offshore Mechanics and Arctic Engineering, June 2015, Vol. 137 / 032001-7, DOI: 10.1115/1.4029999.
2. Bihs H. (2011): Three-Dimensional Numerical Modeling of Local Scouring in Open Channel Flow. PhD thesis, Norwegian University of Science and Technology, Trondheim.
3. Bihs H. (2015a): REEF3D :: User Guide v15.04
4. Bihs H (2015b): DIVEMesh :: User Guide v15.04
5. Berthelsen P. A., Faltinsen O. M. (2008): A local directional ghost cell approach for incompressible viscous flow problems with irregular boundaries. Journal of Computational Physics, 227:4354-4397.
6. Chella M. A., Bihs H., Myrhaug D. (2015): Characteristics and profile asymmetry properties of waves breaking over an impermeable submerged reef. Coastal Engineering 100 (2015) 26-36.
7. Chorin A. (1968): Numerical solution of the Navier Stokes equations. Math. Comput. 22, 745-762.
8. Federal Highway Administration (2008): Highways in the Coastal Environment, Hydraulic Engineering Circular No. 25 (2nd ed.)
9. Dramais G., Le Coz J., Camenen B., Hauet A. (2011): Advantages of a mobile LSPIV method for measuring flood discharges and improving stage-discharge curves, Journal of Hydro-environment Research 5 (2011) 301-312.
10. Fleit G. (2013): Élőhely szempontú folyószabályozás megalapozása korszerű hidromorfológiai adatelemzéssel, BME VVT, TDK dolgozat, Budapest.
11. Fleit G. (2014a): Hajók keltette hullámzás hatásának terepi feltárása a litorális zónában, BME VVT, TDK dolgozat, Budapest.
12. Fleit G. (2014b): Élőhely szempontú folyószabályozás támogatása korszerű terepi mérésekkel és számítógépes modellezéssel, BME VVT, TDK dolgozat, Budapest.
13. Fleit G. (2015): Numerical modeling of complex free surface flows. BSc Thesis, Budapest University of Technology and Economics, Norwegian University of Science and Technology, Trondheim.
14. Gabel F. (2012): Impacts of ship-induced waves on benthic macroinvertebrates. PhD Thesis, Landwirtschaftlich-Gärtnerischen Fakultät der Humboldt-Universität zu Berlin.
15. Hirt C. and Nochols B. (1981): Volume of fluid (VOF) method for the dynamics of free boundaries. Journal of Computational Physics, 39:201-225.
16. Homoródi K., Józsa J., Krámer T., Ciraolo G., Nasello C. (2012): Identifying wave and turbulence components in wind-driven shallow basins, Per. Pol. Civil Eng. 56/1 (2012) 87-95, doi: 10.3311/pp.ci.2012-1.10.
17. Jesson M. (2015): MAJ's Velocity Signal Analyser :: Installation and User Guide v.1.5.46.
18. Jiang G. S., Shu C. W. (1996): Efficient implementation of weighted ENO schemes. J. Comput. Phys. 126, 202-228.
19. Jodeau M., Hauet A., Le Coz J. (2013): Fudaa-LSPIV 1.3.2 - User guide (version v03 08-15-2013).
20. Jolliffe I. T. (1986): Principal Component Analysis. Springer-Verlag. doi:10.1007/b98835. ISBN 978-0-387-95442-4.
21. Jonsson I. G. (1966): Wave boundary layers and friction factors. Proceedings of the 10th International Conference on Coastal Engineering, Tokyo, Japan, ASCE, pp 127–148.
22. Józsa J., Baranya S., Török G., Fleit G. (2014): Duna Sződliget környéki (1672-1676 fkm szelvények közötti) szakaszának természetvédelmi célú átalakítását megalapozó vizsgálatok terepi mérésekkel és számítógépes modellezéssel, DANUBEPARKS STEP 2.0 SEE/D/0165/2.3/X.

23. Krouzecky N., Fenton J.D., Huber B., Klasz G. (2013): Investigations of ship-induced waves on the Austrian Danube in the Donau-Auen National Park. 5th Symposium for Research in Protected Areas 10 to 12 June 2013, Mittersil pages 425-430.
24. Kucera-Hirzinger V., Schludermann E., Zornig H., Weissenbacher A., Schabuss M., Schiemer F. (2009): Potential effects of navigation-induced wave wash on the early life history stages of riverine fish. Aquatl Sci. 71 (2009) 94-102, 1015-1621/09/010094-9, DOI 10.1007/s00027-008-8110-5.
25. Liedermann M., Tritthart M., Hoyer H., Schludermann E., Keckeis H., Habersack H. (2009): Effects of vessel-induced waves on different bank types and their impact on the 0+ fish fauna. 7th ISE & 8th HIC, Chile.
26. Massel S. R. (1996): Ocean surface waves: their physics and prediction, World Scientific.
27. Masselink G., Puleo J. A. (2006): Swash-zone morphodynamics, Continental Shelf Research 26 (2006) 661-680.
28. Muste M., Fujita I., Hauet A. (2008): Large-Scale Particle Image Velocimetry for measurements in riverine environments. Water Resources Research Vol. 44(4).
29. Nortek (2013): Aquadopp Profiler. TS-031-en-06.2013
30. Osher S., Sethian J. A. (1988): Fronts propagating with curvature-dependent speed: algorithms based on Habilton-Jacobi formulations. J. Comput. Phys. 79, 12-49.
31. Pasternack G. B., Bounrisavong M. K., Parikh K. K. (2008): Backwater control on riffle-pool hydraulics, fish habitat quality and sediment transport regime in gravel-bed rivers, Journal of Hydrology, 357, 125-139.
32. Raubenheimer B., Elgar S., Guza R.T. (2004): Observations of swash zone velocities: A note of friction coefficients, Journal of Geophysical Research 109.
33. Reynolds O. (1895): On the Dynamical Theory of Incompressible Viscous Fluids and the Determination of the Criterion. Philosophical Transactions of the Royal Society of London. A, v. 186, pp. 123-164.
34. Shu C. W., Osher S. (1988): Efficient implementation of essentially non-oscillatory shock capturing schemes. J. Comput. Phys. 77, 439-471.
35. Soulsby R. L., and Dyer K. R. (1981): The form of the near-bed velocity profile in a tidally accelerating flow. J. Geophys. Res., 86,8067–8074.
36. U.S. Army Corps of Engineers (2002): Coastal Engineering Manual – Part II, Chapter – Water Waves mechanics. EM 1110-2-1100 (Part II).
37. van der Vorst H. (1992): BiCGStab: a fast and smoothly converging variant of Bi-CF for the solution of nonsymmetric linear systems. SIAM J. Sci. Stat. Comput. 13, 631-644.
38. Wilcox D. C. (1994): Turbulence Modeling for CFD. DCW Industries Inc., La Canada, California.
39. Zeng J., Constantinescu G., Weber L. (2005): A fully 3D Non-Hydrostatic Model for Prediction of Flow, Sediment Transport and Bed Morphology in Open Channels, Proceedings of the 31st IAHR Congress, pp. 1327-1338.